should be noted that the late endosome and lysosome share many features and both endosomal and lysosomal fractions are usually positive for LAMP2. The endosomal fraction isolated by our method contains both early and late endosomes because this fraction was positive for Rab5 and LAMP-2. In this study, the Rab5-negative, LAMP-2 positive component was defined as the lysosomal fraction. These findings suggest that in VPS35-depleted cells, the retromer fails to retrieve CI-MPR from the endosomes, resulting in the accumulation of CI-MPR in the lysosomes. CTSD was detected in both the endosome and lysosome fractions in HEK293 cells. However, after *VPS35* was silenced, the level of mature CTSD was substantially decreased in the lysosomes, whereas the pro-CTSD was upregulated in the endosomes. It is also interesting to note

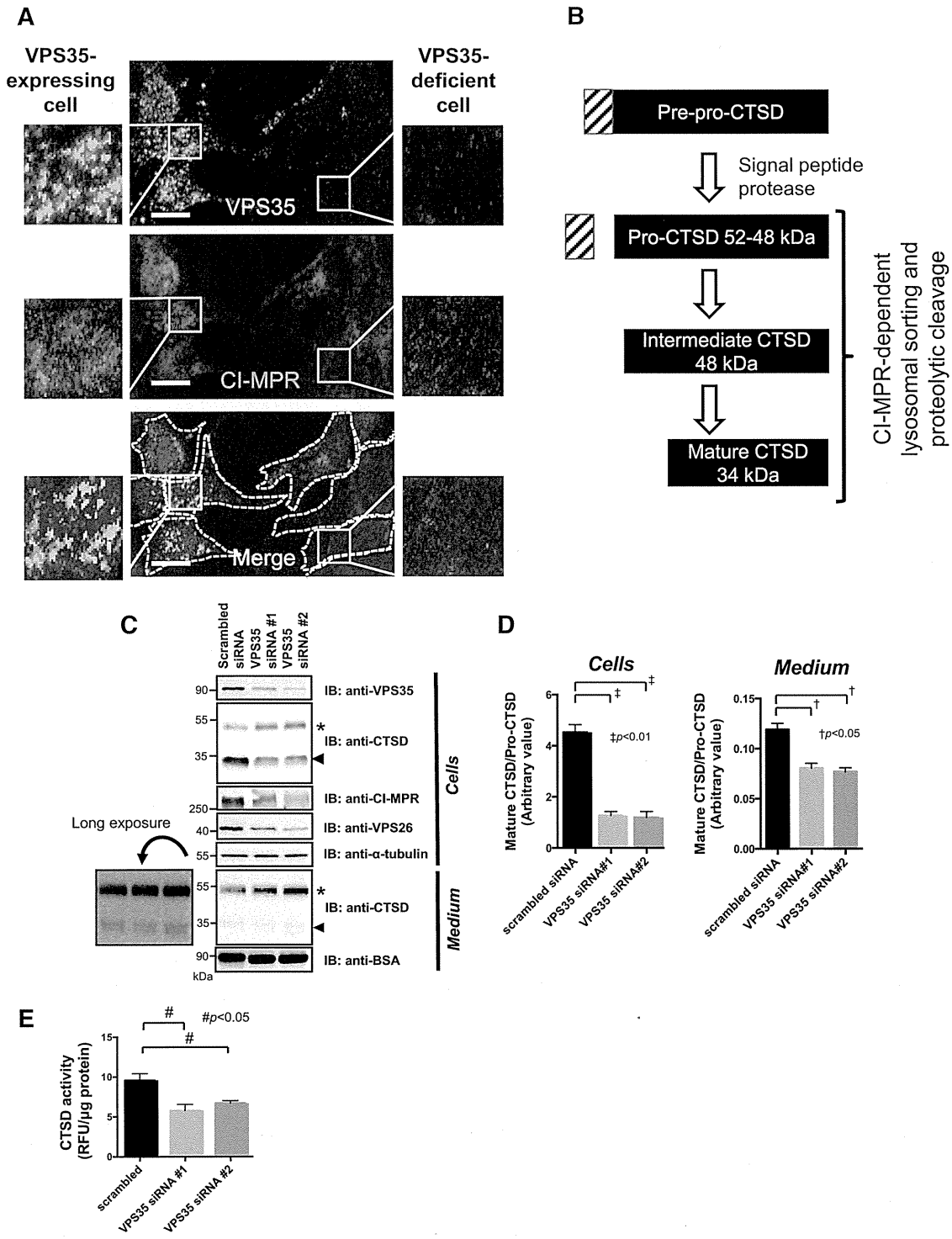

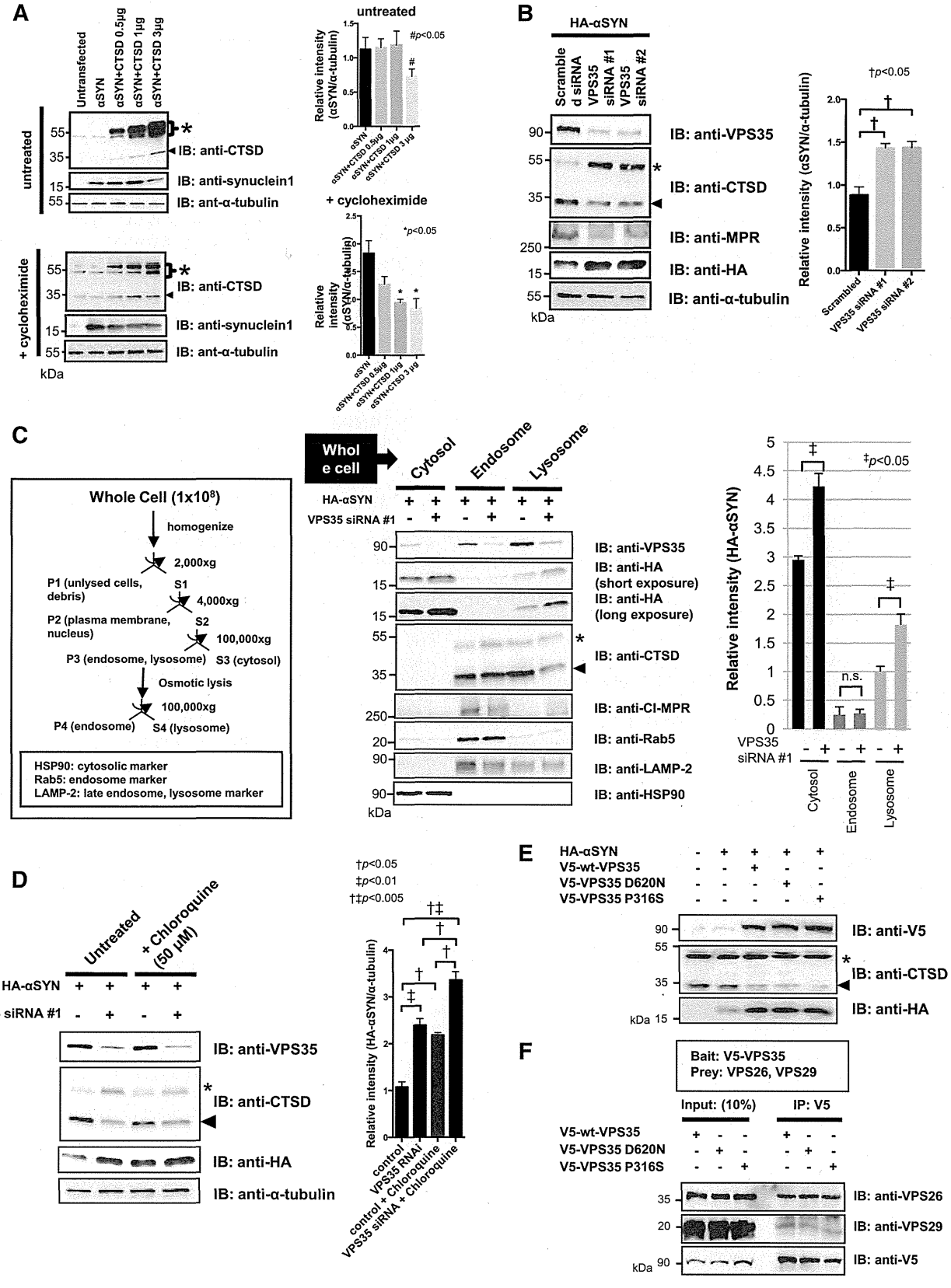
A
Untransfected
αSYN
αSYN+CTSD 0.5μg
αSYN+CTSD 1μg
αSYN+CTSD 3μg
untreated
IB: anti-CTSD
IB: anti-synuclein1
IB: ant-α-tubulin
+ cycloheximide
kDa
untreated
Relative intensity (αSYN/α-tubulin)
#p<0.05
+ cycloheximide
*p<0.05
B
HA-αSYN
Scrambled siRNA
VPS35 siRNA #1
VPS35 siRNA #2
IB: anti-VPS35
IB: anti-CTSD
IB: anti-MPR
IB: anti-HA
IB: anti-α-tubulin
kDa
†p<0.05
Relative intensity (αSYN/α-tubulin)
Scrambled
VPS35 siRNA #1
VPS35 siRNA #2
C
Whole Cell (1x10⁸)
homogenize
2,000xg
P1 (unlysed cells, debris)
S1
4,000xg
P2 (plasma membrane, nucleus)
S2
100,000xg
P3 (endosome, lysosome)
S3 (cytosol)
Osmotic lysis
100,000xg
P4 (endosome)
S4 (lysosome)
HSP90: cytosolic marker
Rab5: endosome marker
LAMP-2: late endosome, lysosome marker
Whole cell
Cytosol
Endosome
Lysosome
HA-αSYN
VPS35 siRNA #1
IB: anti-VPS35
IB: anti-HA (short exposure)
IB: anti-HA (long exposure)
IB: anti-CTSD
IB: anti-CI-MPR
IB: anti-Rab5
IB: anti-LAMP-2
IB: anti-HSP90
kDa
‡p<0.05
Relative intensity (HA-αSYN)
n.s.
VPS35 siRNA #1
Cytosol
Endosome
Lysosome
D
Untreated
+ Chloroquine (50 μM)
HA-αSYN
VPS35 siRNA #1
IB: anti-VPS35
IB: anti-CTSD
IB: anti-HA
IB: anti-α-tubulin
†p<0.05
‡p<0.01
††p<0.005
Relative intensity (HA-αSYN/α-tubulin)
control
VPS35 RNAi
control + Chloroquine
VPS35 siRNA + Chloroquine
E
HA-αSYN
V5-wt-VPS35
V5-VPS35 D620N
V5-VPS35 P316S
IB: anti-V5
IB: anti-CTSD
IB: anti-HA
kDa
F
Bait: V5-VPS35
Prey: VPS26, VPS29
Input: (10%)
IP: V5
V5-wt-VPS35
V5-VPS35 D620N
V5-VPS35 P316S
IB: anti-VPS26
IB: anti-VPS29
IB: anti-V5
kDa

that treatment with chloroquine, a lysosomotropic agent that prevents endosomal acidification, further augmented the accumulation of HA-αSYN by VPS35 RNAi (Fig. 2D). This indicates that VPS35 knockdown does not completely inhibit lysosomal αSYN degradation. These observations indicate that if the retromer machinery is compromised, the pro-CTSD is entrapped in upstream structures and cannot be properly transported to the downstream acidic compartment. In an inverse correlation with the level of mature CTSD, the level of HA-αSYN was substantially upregulated in the lysosome fraction and the cytosol in the *VPS35*-silenced cells. Since autophagosomes should engulf cytosolic αSYN (Vogiatzi et al., 2008), increased cytosolic αSYN can be interpreted as the result of insufficient autophagic/lysosomal clearance of αSYN. To determine the possible effects of PD-linked mutations of *VPS35* on retromer function and αSYN degradation, we co-expressed HA-αSYN and mutant VPS35 (D620N and P316S) in HEK293 cells. Surprisingly, the over-expressed wt and the mutant VPS35 led to an equal αSYN accumulation, with no significant difference in the impaired maturation of CTSD (Fig. 2E). Furthermore, coimmunoprecipitation analyses of the wt and mutant VPS35 detected no differences in the binding affinity toward its known binding partners, VPS26 and VPS29 (Fig. 2F). Together, these findings indicate the essential role of the retromer machinery in lysosomal CTSD function in regulating the proteolytic pathway that is important for αSYN metabolism.

RNAi-mediated silencing of dVPS35 not only increased the insoluble αSYN species in brain but also deteriorated eye organization and locomotor function in human αSYN transgenic Drosophila

Although the retromer is implicated in PD pathogenesis, there is no evidence showing that deficiencies in the retromer sorting pathway cause the key phenotypes of the disease. Because the retromer complex is highly conserved and homologs have been found in yeast, nematode, fly, mouse, and human (Korolchuk et al., 2007), we investigated the effects of endogenous VPS35 on αSYN-induced neurotoxicity using flies that express the *h[wt]-SNCA* and *dVPS35* RNAi transgenes. The sequence-specific silencing of *dVPS35* in the fly brain was confirmed by RT-PCR (Fig. 3A). We found that the silencing of *dVPS35* strikingly increased the amount of the Triton-insoluble high-molecular-weight (HMW) αSYN species accompanied by a concomitant reduction in the level of Triton-soluble αSYN monomer in the brains of human αSYN-expressing flies under the panneural *embryonic lethal abnormal vision* (*elav*)-GAL4 driver (Fig. 3B). This finding is well corroborated by the immunohistochemical findings showing that the numbers of αSYN-positive inclusions in the fly cortex (Kenyon cells) were significantly increased in the brain of VPS35-deficient flies compared to controls (Fig. 3C). We attempted to detect human αSYN in the fly brain with or without proteinase K treatment, but did not observe a significant difference (data not shown). The mRNA levels in the brain of 4 fly lines were analyzed by RT-PCR (Fig. 3D). Note that the transcript levels of *h[wt]-SNCA* versus *rp49* were statistically identical between the *h[wt]-SNCA* × *GFP* RNAi and *h[wt]-SNCA* × *dVPS35* RNAi-1 fly lines. Furthermore, the cathepsin D activity in the brain was significantly decreased in *dVPS35* depleted flies (Fig. 3E). We then analyzed the eye phenotypes of flies expressing αSYN under the eye-specific *glass multiple reporter* (*GMR*)-GAL4 driver (Fig. 4A and B). When *dVPS35* was silenced, the human αSYN-Tg flies showed a slight shrinkage of each ommatidium with the loss of interommatidial bristles compared to control flies expressing both *h[wt]-SNCA* and *GFP* RNAi or both *EGFP* and *dVPS35* RNAi. We then investigated the impact of *dVPS35* silencing on the motor performance of flies that over-expressed human αSYN in the nervous system. For this purpose, we utilized a simple but powerful behavioral assay: the climbing assay. As shown in Fig. 5A and B, the flies overexpressing human wt-αSYN with *dVPS35* RNAi (*dVPS35* RNAi-1 and *dVPS35* RNAi-2) showed a significant, age-dependent deterioration in climbing ability compared to those expressing *GFP*-RNAi. Note that the flies that expressed αSYN in the absence of *dVPS35* did not have a shortened life span compared to the control flies (data not shown).

Discussion

In this study, we first showed that the silencing of *VPS35* in cultured cells caused a reduction in the distribution of CI-MPR and impaired the maturation of CTSD. Second, we found that the amount of pro-CTSD was substantially increased in the culture medium of the VPS35-deficient cells. Third, we demonstrated that silencing *VPS35* impairs the maturation of CTSD, which occurs concomitant with a striking accumulation of αSYN in lysosomes. Finally, we showed that the RNAi-mediated silencing of *dVPS35* not only induced the accumulation of the detergent-insoluble αSYN species in the brain but also exacerbated mild eye disorganization, as well as causing locomotor impairment in the flies expressing the human wild-type αSYN. Cumulatively, these data suggest that the retromer-dependent sorting machinery plays a role in αSYN catabolism by modulating the intracellular processing and activation of CTSD and might thereby contribute to the pathogenesis of PD (Fig. 6).

Although the evidence suggests that VPS35 is involved in the pathogenesis of PD, the mechanisms by which the mutant VPS35 causes retromer dysfunction and the subsequent neurodegeneration remain elusive. Given that the expression of VPS35 is significantly decreased in the brain regions selectively vulnerable to PD and AD and the studies in animal models (MacLeod et al., 2013; Muhammad et al., 2008; Small et al., 2005; Wen et al., 2011), the loss-of-function mechanism may explain the VPS35-related defective vesicle trafficking and subsequent neurodegeneration. As suggested by previous studies, our immunoprecipitation analyses indicate that the over-expressed VPS35 mutants (D620N and P316S) seem to maintain the binding capacity for the retromer subunits VPS26 and VPS29 (Vilarino-Guell et al., 2011). Nevertheless, the expression of the yeast VPS35 mutation (p.R98W) in the

Fig. 2. VPS35 depletion impairs the maturation of CTSD concomitantly with the accumulation of αSYN mainly in the late endosomes and lysosomes. (A) The level of exogenously expressed human αSYN (17 kDa) in HEK293 cells was decreased when the CTSD was highly over-expressed (3 μg plasmid for transfection) for 48 h (upper panel). Notably, under the existence of protein synthesis inhibitor cycloheximide, the effect of CTSD on αSYN degradation was augmented and the amount of αSYN was significantly decreased in proportion to the dosage of CTSD expression (lower panel). Pro-CTSD and mature CTSD are indicated by an asterisk and an arrowhead, respectively. Representative immunoblots from three independent experiments are shown. The densitometric quantification of αSYN versus α-tubulin is presented in the right panel. Data are expressed as the means ± standard errors. $^{\#,*}p < 0.05$ (one-way ANOVA followed by Dunnett's test; $n = 5$). (B) The depletion of VPS35 by siRNA (#1 and #2) induced the accumulation of intracellular HA-αSYN concomitant with the incorrect processing of CTSD in HEK293 cells stably expressing HA-αSYN. Pro-CTSD and mature CTSD are indicated by an asterisk and an arrowhead, respectively. Retromer dysfunction in VPS35-deficient cells was confirmed by the reduction in CI-MPR expression. Representative immunoblots from three independent experiments are presented. The relative band intensity of αSYN versus α-tubulin was calculated and is presented in the right panel. Data are expressed as the means ± standard errors. $^{\dagger}p < 0.05$ (one-way ANOVA followed by Dunnett's test; $n = 5$). (C) A marked increase in HA-αSYN in the lysosome fraction, as well as the cytosol, in *VPS35*-silenced HEK293 cells expressing HA-αSYN. Note that the expression level of CI-MPR was slightly decreased in the endosomes but simultaneously increased in the downstream lysosome compartments. CTSD was detected both in the endosome and lysosome fractions in HEK293 cells; however, after silencing *VPS35*, the level of mature CTSD (arrowhead) was substantially decreased in the lysosomes, whereas the pro-CTSD (asterisk) appeared upregulated in the endosomes. HSP90, Rab5, and LAMP-2 were used as the subcellular markers for the cytosol, endosome, and late endosome/lysosome, respectively. The fractionation and immunostaining were performed five times and exhibited consistent results. The densitometric quantification of HA-αSYN in each fraction is presented in the right panel. Data are expressed as the means ± standard errors. $^{\ddagger}p < 0.05$ (unpaired Student's *t*-test; $n = 5$). (D) Treatment with the lysosomal inhibitor, chloroquine (50 μM for 5 h), significantly augmented the accumulation of HA-αSYN by VPS35 RNAi. The relative band intensity of HA-αSYN versus α-tubulin is presented in the right panel. Data are expressed as the means ± standard errors. $^{\dagger}p < 0.05$ and $^{\ddagger}p < 0.01$ (one-way ANOVA followed by Dunnett's test; $n = 5$). (E) The over-expressed wt as well as mutant VPS35 in HEK293 cells equally led to αSYN accumulation, with no significant difference in the impaired CTSD maturation. (F) Coimmunoprecipitation analyses using HEK293 cells co-expressing wt and the mutant VPS35 detected no difference in the binding affinity toward its known binding partners, VPS26 and VPS29. Experiments were performed 3 times and yielded similar results.

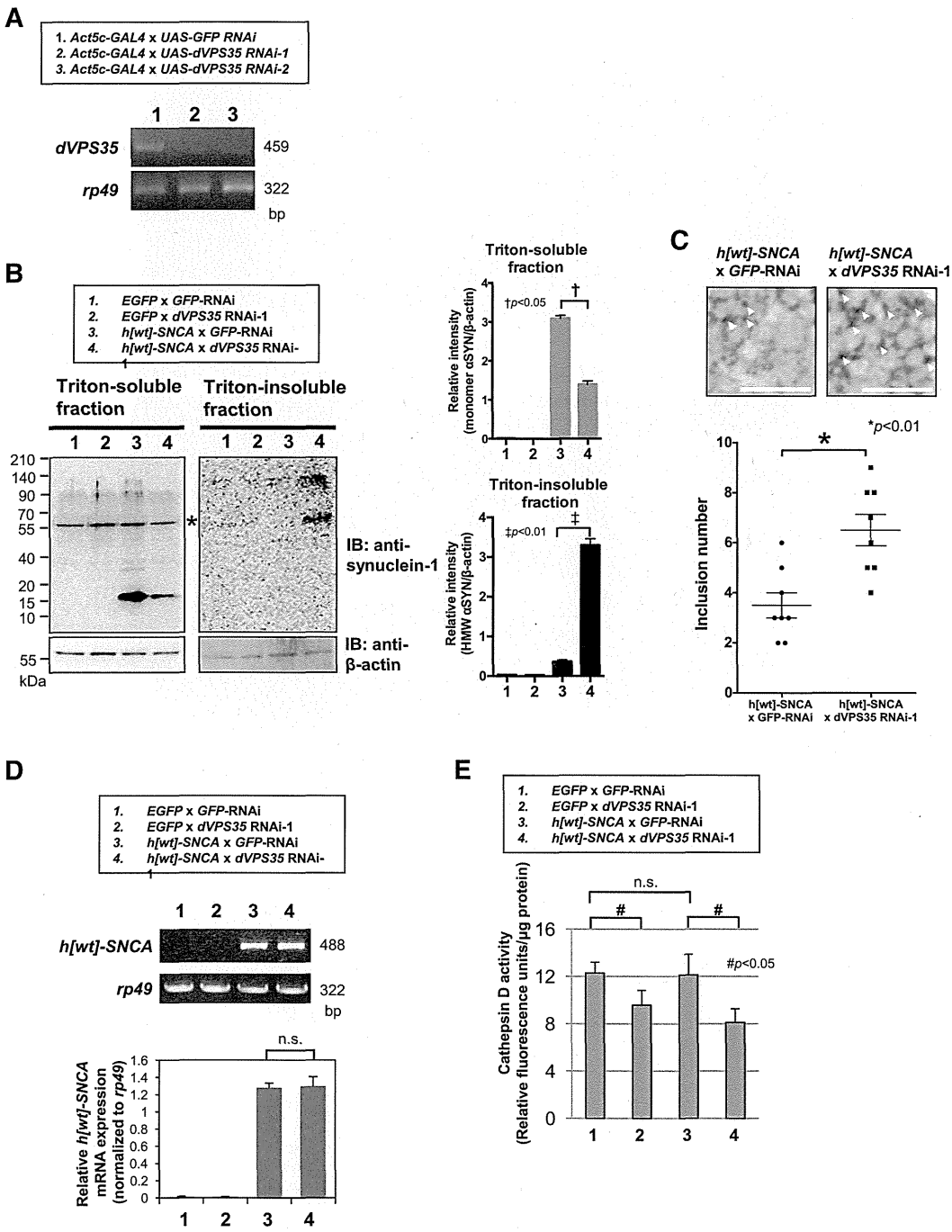

Fig. 3. Knockdown of *dVPS35* in human αSYN transgenic *Drosophila*. (A) Generation of *dVPS35*-knockdown flies. The sequence-specific silencing of *dVPS35* in the fly brain was confirmed by RT-PCR analysis. Ribosomal protein 49 (*rp49*), a housekeeping gene, was used as an internal control. RNAi-mediated knockdown was induced by *Act5c*-GAL4, which expresses GAL4 ubiquitously. (B) Neuron-specific knockdown of *dVPS35* affects the catabolism of the human wt αSYN. The *elav*-GAL4 driver was used for the transgene expression. Note that the silencing of *dVPS35* strikingly increased the amount of Triton-insoluble HMW αSYN species, which was accompanied by the concomitant reduction in Triton-soluble αSYN monomer in the brains of human αSYN-expressing flies under the *elav*-GAL4 driver. Equal loading was confirmed by an immunoblot using a β-actin Ab. An asterisk indicates the unspecific band that emerged due to the synuclein-1 Ab. The normalized band intensity data of monomeric αSYN in the Triton-soluble fraction (gray bar) as well as the HMW αSYN (above 100 kDa) in the Triton-insoluble fraction (black bar) are presented in the right panel. Data are expressed as the means ± standard errors. $^{\dagger}p < 0.05$ and $^{\ddagger}p < 0.01$ (one-way ANOVA followed by Dunnett's test; $n = 5$). (C) The immunohistochemical staining of fly brains using a human αSYN-specific antibody. The αSYN-positive inclusions (arrowhead) were counted in a defined area of the cortex (Kenyon cell). Note that the numbers of αSYN-positive inclusions in the fly cortex were significantly increased in the brain of VPS35-deficient flies compared to controls. Scale bar: 10 μm. (D) The mRNA levels in the brains of 4 fly lines were analyzed by RT-PCR. *Rp49* was used as an internal control. Note that the transcript levels of *h[wt]-SNCA* are statistically identical between the *h[wt]-SNCA* × *GFP* RNAi and *h[wt]-SNCA* × *dVPS35* RNAi-1 fly lines. The relative *h[wt]-SNCA* mRNA expression levels normalized to *rp49* were calculated. Data are expressed as the means ± standard errors (one-way ANOVA followed by Dunnett's test; $n = 5$). (E) The CTSD activity in the brain was significantly decreased in *dVPS35* depleted flies. Results are presented as means ± standard errors. $^{\#}p < 0.05$ (one-way ANOVA with the post-hoc Dunnett's test; $n = 5$).

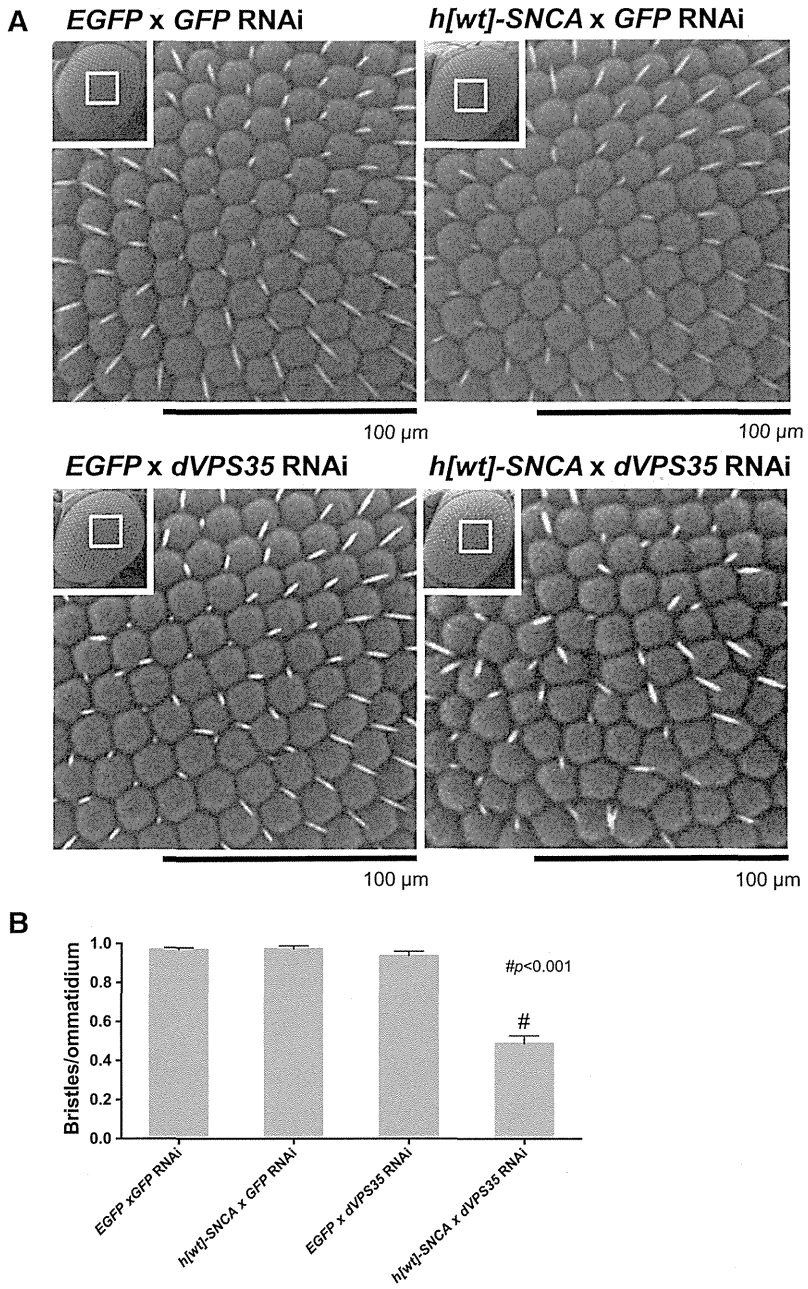

Fig. 4. Silencing of *dVPS35* induces mild eye disorganization in human αSYN transgenic *Drosophila*. (A) Eye-specific expression of *h[wt]-SNCA* with *dVPS35* RNAi resulted in compound eye disorganization. The eye phenotype was normal in 1-week-old transgenic flies over-expressing *h[wt]-SNCA* with *GFP* RNAi. By contrast, when *dVPS35* was silenced, the *h[wt]-SNCA*-Tg flies showed a slight shrinkage of each ommatidium with disarrayed bristles compared to the control flies expressing both *h[wt]-SNCA* and *GFP* RNAi or both *EGFP* and *dVPS35* RNAi. The white square indicates the magnified area. Scale bar: 100 μm. (B) For the quantification of intact interommatidial bristle numbers, the number of visible bristles was counted and divided by the total number of ommatidium. Note that the silencing of dVPS35 in SNCA transgenic flies significantly decreased the numbers of bristles compared to other fly lines. The pooled data were statistically analyzed by a one-way ANOVA followed by a Bonferroni multiple comparison test. $^{\#}p < 0.001$ ($n \geq 10$).

highly conserved PRLYL motif at the N-terminus destabilizes VPS26 and disrupts cargo sorting in the prevacuolar endosome and retrieval of the retromer to the TGN, indicating that this mutation converts VPS35 to a dominant-negative protein in *Saccharomyces cerevisiae* (Zhao et al., 2007). Similarly, in a rat insulinoma cell line, the exogenous expression of the human VPS35 R107W mutant (the functional equivalent of the R98 residue in yeast) has an altered intracellular membrane distribution that perturbs a number of post-Golgi trafficking functions (Zhao et al., 2007). Moreover, a recent study has shown that the expression of D620N VPS35 induces the marked degeneration of dopaminergic neurons both in primary neuron culture and in a rat model (Tsika et al., 2014). These findings suggest that mutant VPS35 may have an influence on retromer function via a potentially toxic gain-of-function with a dominant negative effect. This notion is supported by a recent observation demonstrating that the PD-linked *VPS35* D620N mutation disrupts the cargo-sorting function of the retromer, causing an abnormal trafficking of CTSD (Follett et al., 2014). We also produced the overexpression of the PD-linked mutant VPS35 (D620N and P316S) in

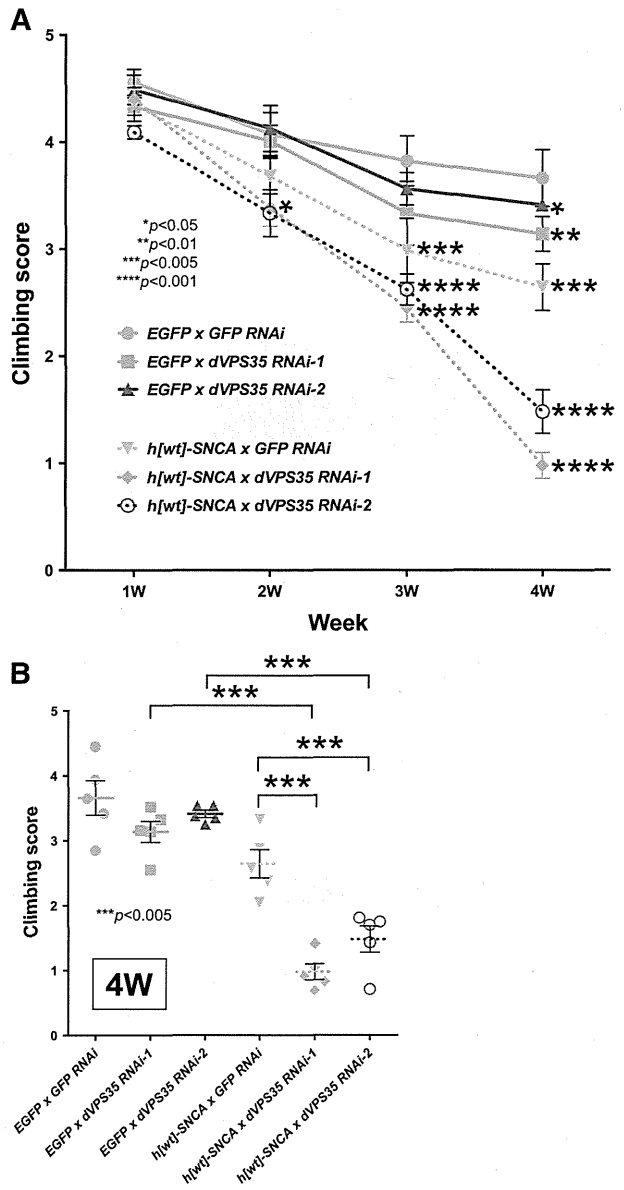

Fig. 5. RNAi-mediated silencing of *dVPS35* deteriorates locomotor function in human αSYN transgenic *Drosophila*. (A) Knockdown of *dVPS35* induced an age-dependent decline in climbing performance in flies expressing the human αSYN in the nervous system. Five trials were performed in each group at 20 s intervals and the climbing index was calculated. Results are presented as the means ± standard errors of the scores obtained in 5–10 independent experiments. All climbing assay experiments were conducted at 25 °C. The *Elav*-GAL4 driver was used for the experiment. (B) In order to make it easier to compare each climbing performance in different fly lines, the climbing scores of 4-week-old flies are also presented as a categorized scatter plot with mean segments. Pooled data from at least 5 experiments were statistically analyzed. $^{*}p < 0.05$, $^{**}p < 0.01$, $^{***}p < 0.005$, and $^{****}p < 0.001$ (two-way ANOVA with the Bonferroni multiple comparison test; $n \geq 5$).

HEK293 cells to determine its distinct influence on retromer function. Unexpectedly, not only the exogenously expressed mutants, but also the wt VPS35 equally resulted in the aberrant trafficking of CI-MPR together with the impaired maturation of CTSD. This finding is apparently contradictory to a report by Follett et al., which demonstrated that exogenous expression of the mutant D620N, but not the wt VPS35, abnormally traffics CI-MPR in HEK293 cells, resulting in the incorrect processing of CTSD. Although the reasons for these discrepancies are not clear, a possible explanation is the difference in the protein expression level in each experiment. The retromer requires an apparent equimolar stoichiometry of the subunit to exert its normal function (Hierro et al., 2007; Seaman et al., 2009). Thus, it is possible that even the wt VPS35 may be able to negatively perturb the function of the retromer when heavily over-expressed.

Regardless of the modes of gene action, the genetic modification of VPS35 can result in the disruption of retromer function and the aberrant trafficking of cargo proteins such as CI-MPR. CI-MPR appears to be the primary receptor for the major lysosomal 'α-synucleinase' CTSD that is abundantly expressed in the brain (Ludwig et al., 1994; Press et al., 1998). Indeed, Sevlever et al. found that the main degradation activity of αSYN in the lysosomal fractions from cultured neurons was greatly inhibited by the CTSD inhibitor pepstatin A (Sevlever et al., 2008). They showed that other protease inhibitors such as leupeptin weakly reduced αSYN degradation. This result indicates that in addition to CTSD, other proteolytic activities play a role in αSYN degradation within lysosomes. This notion is corroborated by our data showing that treatment of the lysosomal inhibitor chloroquine slightly but significantly augmented αSYN levels in cells transfected with VPS35 siRNA. Nevertheless, the altered processing and prominent accumulation of insoluble species of endogenous αSYN in three different mammals with CTSD deficiency indicate that its enzyme activity plays a fundamental role in αSYN metabolism (Cullen et al., 2009). Although both the proteasome and the lysosome have been proposed to play a role in the degradation of αSYN (Ebrahimi-Fakhari et al., 2011; Konno et al., 2012), recent observations have underscored the contribution of the autophagy–lysosome pathway (Mak et al., 2010; Vogiatzi et al., 2008). CTSD, lysosome-associated membrane protein-1 (LAMP-1), and heat shock protein 73 (Hsp73) immunoreactivities are significantly decreased (approximately 50% versus control) in the substantia nigra neurons of idiopathic PD patients (Chu et al., 2009). Furthermore, parkinsonism has been noted in lysosomal deficiencies such as the adult forms of neuronal ceroid lipofuscinosis, Gaucher disease, and Kufor–Rakeb syndrome (Schneider and Zhang, 2010). The CTSD deficiency is thought to broadly influence the lysosomal and autophagic degradation of its substrate proteins (Koike et al., 2000). Moreover, recent work has revealed that the D620N mutant VPS35 fails to associate with the WASH (Wiskott–Aldrich syndrome protein and SCAR homolog) complex, an important regulator of vesicle trafficking. This failure impairs the autophagic clearance of huntingtin proteins with Q74 repeats and the A53T mutant of αSYN (Zavodszky et al., 2014), raising the question of how the impaired autophagic–lysosomal degradation by retromer dysfunction can specifically lead to αSYN accumulation. One possible mechanism is the involvement of the chaperone-mediated autophagy (CMA). Indeed, the amino acid sequence of αSYN contains a pentapeptide succession consistent with a CMA recognition motif and *in vitro* experiments demonstrated that this motif is essential for the internalization of αSYN into the lysosomal lumen and for degradation by lysosomal proteases (Cuervo et al., 2004). Another regulatory mechanism which may control the selective sorting and degradation of αSYN in lysosomes is the ubiquitin-modification. It has been shown that Nedd4 (neural precursor cell expressed developmentally down-regulated protein 4), a ubiquitin E3 ligase that targets protein substrates to lysosomes, catalyzes K63-mediated αSYN ubiquitination and enhances its clearance in lysosomes (Sugeno et al., 2014; Tofaris et al., 2011). Moreover, the over-expression of wt-Nedd4 reduces αSYN accumulation in the nervous tissue and induces neurodegeneration and locomotor abnormality in both fly and rat models (Davies et al., 2014). This finding is well corroborated by the yeast model experiment showing that N-aryl benzimidazole (NAB) strongly and selectively counteracts the αSYN cytotoxicity through its influence on Rsp5, a yeast homolog of Nedd4 (Tardiff et al., 2013). Our experiments using a novel fly model of VPS35-linked PD provide evidence for a modulatory effect of endogenous VPS35 expression on αSYN toxicity *in vivo*. Despite the lack of direct evidence showing that fruit fly CTSD accepts human αSYN as a substrate, we found that the knockdown of dVPS35 significantly

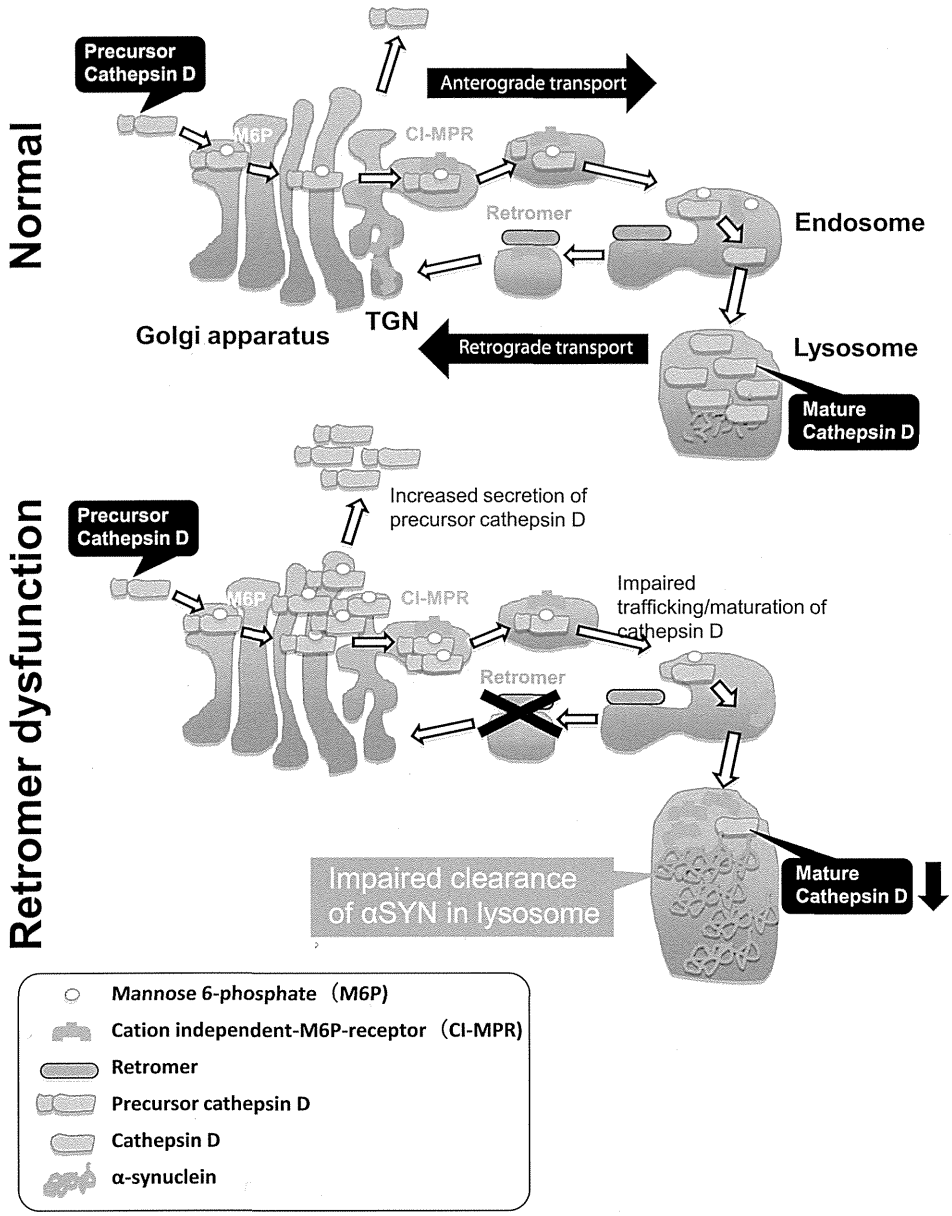

Fig. 6. Schematic illustrations of retromer-mediated trafficking of CTSD and possible contribution to lysosomal αSYN degradation. VPS35, a critical component of the retromer complex, mediates retrograde transport of cargo protein (CI-MPR) from endosome to the TGN. Under physiological condition (upper panel), upon arrival in the Golgi apparatus, newly synthesized CTSD precursor is specifically modified with M6P residues, which are recognized by CI-MPR in the TGN. CI-MPR escorts CTSD into endosomes, in which the CTSD are released for further transport to lysosomes. During this process, CTSD is activated by the proteolytic cleavage of the signal peptide sequence. The retromer retrieves the unoccupied MPRs from endosomes to the TGN, where they participate in further cycles of CTSD sorting. If the retromer function is perturbed (lower panel), the retromer fails to retrieve CI-MPR from the endosome to the TGN, which results in increased secretion of precursor CTSD as well as the impaired trafficking of CTSD. As a consequence, the amount of mature CTSD in the lysosome is decreased, which increases the accumulation of αSYN and might influence the neurodegenerative process linked to PD.

lowered the CTSD activity in fly brain and the deletion of the homologous CTSD-encoding gene in the fly promoted the toxicity of the ectopically expressed human αSYN in the fly retina (Cullen et al., 2009). These observations suggest that the altered expression level of dVPS35 may interfere with CTSD activation and thereby have an effect on the cellular burden of αSYN. Indeed, the accumulation of the HMW Triton-insoluble αSYN species accompanied by a decrease in soluble monomeric αSYN in our fly model is consistent with the results in CTSD-deficient mouse brain showing that the level of soluble endogenous αSYN was reduced, whereas the levels of insoluble, oligomeric αSYN species were increased (Cullen et al., 2009). The reason that the αSYN monomer was decreased in the dVPS35-deficient fly brain whereas the monomeric αSYN was increased in VPS35-silenced HEK293 cells is uncertain. However, it is possible that the long-lasting CTSD deficiency caused by retromer malfunction may facilitate the buildup of the HMW αSYN species. The eye phenotype of the dVPS35-deficient αSYN transgenic fly is relatively mild compared to that of CTSD-knockout flies that showed age-dependent vacuolar degeneration and thinning of the retinal architecture (Cullen et al., 2009). Furthermore, the life span of our flies was roughly comparable to that of normal flies, whereas the CTSD-knockdown flies manifested a clearly shortened life span (Tsakiri et al., 2013). Presumably, there may be an inverse

correlation between the severity of the disease and the level of residual CTSD enzyme activity. The observed mild eye degeneration and the age-dependent decline of motor performance in αSYN Tg flies with a dVPS35-null background may recapitulate the slowly progressive feature of the human disease. Although the underlying molecular mechanism by which VPS35 deficiency facilitates eye disorganization and progressive motor disability in human αSYN Tg flies remains enigmatic, there is substantial evidence to suggest that the toxic conversion of αSYN from soluble monomers to aggregated, insoluble forms in the brain is a key event in the pathogenesis of PD and related diseases (Cookson, 2005). Thus, the intracellular buildup of the potentially noxious αSYN species in the fly brain may partly provide a plausible explanation for the cytotoxicity.

In summary, we found that retromer depletion impaired CTSD maturation in parallel with the accumulation of αSYN in lysosomes. Moreover, the newly established fly model of *VPS35*-linked PD provided evidence for a possible modulatory effect of endogenous VPS35 expression on αSYN toxicity *in vivo*. Interestingly, MacLeod et al. (2013) have demonstrated that wt VPS35 (PARK17) could rescue the phenotypes caused by LRRK2 (PARK8) or RAB7L1 (PARK16) risk variants both *in vitro* and *in vivo*. Furthermore, the locomotor abnormalities and shortened lifespan in flies expressing mutant human LRRK2 can be rescued by the overexpression of VPS35 (Linhart et al., 2014). These findings indicate that these PD-associated genes may configure a common cellular pathway. The functional interrelationship of the endo-lysosomal system in PD is also highlighted by the recent identification of pathogenic mutations in *DNAJC6* and *DNAJC13*, recently identified genes encoding the DNAJ domain-bearing proteins involved in endosomal trafficking, in rare familial forms of PD (Edvardson et al., 2012; Vilarino-Guell et al., 2014). Further studies will be required to gain insight into the pathophysiological role of the endocytosis and endo/lysosomal trafficking systems in synucleinopathy and to identify molecular targets for potential therapeutic interventions.

Acknowledgments

The authors thank Dr. Matthew J. Farrer (Centre of Applied Neurogenetics, University of British Columbia, Canada) for providing the human wt and mutant (D620N and P316S) VPS35 constructs. This work was supported in part by a Grant-in-Aid for Scientific Research (C) [grant number 26461263], a Grant-in-Aid for Scientific Research (B) [grant number 24390219], and a Grant-in-Aid for Exploratory Research [grant number 24659423] from the Ministry of Education, Culture, Sports, Science and Technology (MEXT); a grant from the Research Committee for Ataxic Diseases, a Grant-in-Aid for Scientific Research on Innovative Areas (Brain Environment) [grant number 24111502] from the Ministry of Health, Labor, and Welfare, Japan; and the Intramural Research Grant [grant number 24-5] for Neurological and Psychiatric Disorders of the National Center of Neurology and Psychiatry (NCNP), Japan.

References

Bennett, M.C., Bishop, J.F., Leng, Y., Chock, P.B., Chase, T.N., Mouradian, M.M., 1999. Degradation of alpha-synuclein by proteasome. J. Biol. Chem. 274, 33855–33858.

Capony, F., Rougeot, C., Montcourrier, P., Cavailles, V., Salazar, G., Rochefort, H., 1989. Increased secretion, altered processing, and glycosylation of pro-cathepsin D in human mammary cancer cells. Cancer Res. 49, 3904–3909.

Chen, L., Feany, M.B., 2005. Alpha-synuclein phosphorylation controls neurotoxicity and inclusion formation in a Drosophila model of Parkinson disease. Nat. Neurosci. 8, 657–663.

Chu, Y., Dodiya, H., Aebischer, P., Olanow, C.W., Kordower, J.H., 2009. Alterations in lysosomal and proteasomal markers in Parkinson's disease: relationship to alpha-synuclein inclusions. Neurobiol. Dis. 35, 385–398.

Cookson, M.R., 2005. The biochemistry of Parkinson's disease. Annu. Rev. Biochem. 74, 29–52.

Cuervo, A.M., Stefanis, L., Fredenburg, R., Lansbury, P.T., Sulzer, D., 2004. Impaired degradation of mutant alpha-synuclein by chaperone-mediated autophagy. Science 305, 1292–1295.

Cullen, V., Lindfors, M., Ng, J., Paetau, A., Swinton, E., Kolodziej, P., Boston, H., Saftig, P., Woulfe, J., Feany, M.B., Myllykangas, L., Schlossmacher, M.G., Tyynela, J., 2009. Cathepsin D expression level affects alpha-synuclein processing, aggregation, and toxicity in vivo. Mol. Brain 2, 5.

Davies, S.E., Hallett, P.J., Moens, T., Smith, G., Mangano, E., Kim, H.T., Goldberg, A.L., Liu, J.L., Isacson, O., Tofaris, G.K., 2014. Enhanced ubiquitin-dependent degradation by Nedd4 protects against alpha-synuclein accumulation and toxicity in animal models of Parkinson's disease. Neurobiol. Dis. 64, 79–87.

Dehay, B., Martinez-Vicente, M., Caldwell, G.A., Caldwell, K.A., Yue, Z., Cookson, M.R., Klein, C., Vila, M., Bezard, E., 2013. Lysosomal impairment in Parkinson's disease. Mov. Disord. 28, 725–732.

Ebrahimi-Fakhari, D., Cantuti-Castelvetri, I., Fan, Z., Rockenstein, E., Masliah, E., Hyman, B.T., McLean, P.J., Unni, V.K., 2011. Distinct roles in vivo for the ubiquitin–proteasome system and the autophagy-lysosomal pathway in the degradation of alpha-synuclein. J. Neurosci. 31, 14508–14520.

Edvardson, S., Cinnamon, Y., Ta-Shma, A., Shaag, A., Yim, Y.I., Zenvirt, S., Jalas, C., Lesage, S., Brice, A., Taraboulos, A., Kaestner, K.H., Greene, L.E., Elpeleg, O., 2012. A deleterious mutation in DNAJC6 encoding the neuronal-specific clathrin-uncoating co-chaperone auxilin, is associated with juvenile parkinsonism. PLoS One 7, e36458.

Feany, M.B., Bender, W.W., 2000. A Drosophila model of Parkinson's disease. Nature 404, 394–398.

Follett, J., Norwood, S.J., Hamilton, N.A., Mohan, M., Kovtun, O., Tay, S., Zhe, Y., Wood, S.A., Mellick, G.D., Silburn, P.A., Collins, B.M., Bugarcic, A., Teasdale, R.D., 2014. The Vps35 D620N mutation linked to Parkinson's disease disrupts the cargo sorting function of retromer. Traffic 15, 230–244.

Hasegawa, T., Matsuzaki, M., Takeda, A., Kikuchi, A., Akita, H., Perry, G., Smith, M.A., Itoyama, Y., 2004. Accelerated alpha-synuclein aggregation after differentiation of SH-SY5Y neuroblastoma cells. Brain Res. 1013, 51–59.

Hasegawa, T., Matsuzaki-Kobayashi, M., Takeda, A., Sugeno, N., Kikuchi, A., Furukawa, K., Perry, G., Smith, M.A., Itoyama, Y., 2006. Alpha-synuclein facilitates the toxicity of oxidized catechol metabolites: implications for selective neurodegeneration in Parkinson's disease. FEBS Lett. 580, 2147–2152.

Hasegawa, T., Baba, T., Kobayashi, M., Konno, M., Sugeno, N., Kikuchi, A., Itoyama, Y., Takeda, A., 2010. Role of TPPP/p25 on alpha-synuclein-mediated oligodendroglial degeneration and the protective effect of SIRT2 inhibition in a cellular model of multiple system atrophy. Neurochem. Int. 57, 857–866.

Hasegawa, T., Konno, M., Baba, T., Sugeno, N., Kikuchi, A., Kobayashi, M., Miura, E., Tanaka, N., Tamai, K., Furukawa, K., Arai, H., Mori, F., Wakabayashi, K., Aoki, M., Itoyama, Y., Takeda, A., 2011. The AAA-ATPase VPS4 regulates extracellular secretion and lysosomal targeting of alpha-synuclein. PLoS One 6, e29460.

Hierro, A., Rojas, A.L., Rojas, R., Murthy, N., Effantin, G., Kajava, A.V., Steven, A.C., Bonifacino, J. S., Hurley, J.H., 2007. Functional architecture of the retromer cargo-recognition complex. Nature 449, 1063–1067.

Hilgers, V., Bushati, N., Cohen, S.M., 2010. Drosophila microRNAs 263a/b confer robustness during development by protecting nascent sense organs from apoptosis. PLoS Biol. 8, e1000396.

Koike, M., Nakanishi, H., Saftig, P., Ezaki, J., Isahara, K., Ohsawa, Y., Schulz-Schaeffer, W., Watanabe, T., Waguri, S., Kametaka, S., Shibata, M., Yamamoto, K., Kominami, E., Peters, C., von Figura, K., Uchiyama, Y., 2000. Cathepsin D deficiency induces lysosomal storage with ceroid lipofuscin in mouse CNS neurons. J. Neurosci. 20, 6898–6906.

Konno, M., Hasegawa, T., Baba, T., Miura, E., Sugeno, N., Kikuchi, A., Fiesel, F.C., Sasaki, T., Aoki, M., Itoyama, Y., Takeda, A., 2012. Suppression of dynamin GTPase decreases alpha-synuclein uptake by neuronal and oligodendroglial cells: a potent therapeutic target for synucleinopathy. Mol. Neurodegener. 7, 38.

Korolchuk, V.I., Schutz, M.M., Gomez-Llorente, C., Rocha, J., Lansu, N.R., Collins, S.M., Wairkar, Y.P., Robinson, I.M., O'Kane, C.J., 2007. Drosophila Vps35 function is necessary for normal endocytic trafficking and actin cytoskeleton organisation. J. Cell Sci. 120, 4367–4376.

Laurent-Matha, V., Derocq, D., Prebois, C., Katunuma, N., Liaudet-Coopman, E., 2006. Processing of human cathepsin D is independent of its catalytic function and autoactivation: involvement of cathepsins L and B. J. Biochem. 139, 363–371.

Lee, B.R., Kamitani, T., 2011. Improved immunodetection of endogenous alpha-synuclein. PLoS One 6, e23939.

Linhart, R., Wong, S.A., Cao, J., Tran, M., Huynh, A., Ardrey, C., Park, J.M., Hsu, C., Taha, S., Peterson, R., Shea, S., Kurian, J., Venderova, K., 2014. Vacuolar protein sorting 35 (Vps35) rescues locomotor deficits and shortened lifespan in Drosophila expressing a Parkinson's disease mutant of Leucine-rich repeat kinase 2 (LRRK2). Mol. Neurodegener. 9, 23.

Ludwig, T., Munier-Lehmann, H., Bauer, U., Hollinshead, M., Ovitt, C., Lobel, P., Hoflack, B., 1994. Differential sorting of lysosomal enzymes in mannose 6-phosphate receptor-deficient fibroblasts. EMBO J. 13, 3430–3437.

MacLeod, D.A., Rhinn, H., Kuwahara, T., Zolin, A., Di Paolo, G., McCabe, B.D., Marder, K.S., Honig, L.S., Clark, L.N., Small, S.A., Abeliovich, A., 2013. RAB7L1 interacts with LRRK2 to modify intraneuronal protein sorting and Parkinson's disease risk. Neuron 77, 425–439.

Mak, S.K., McCormack, A.L., Manning-Bog, A.B., Cuervo, A.M., Di Monte, D.A., 2010. Lysosomal degradation of alpha-synuclein in vivo. J. Biol. Chem. 285, 13621–13629.

Muhammad, A., Flores, I., Zhang, H., Yu, R., Staniszewski, A., Planel, E., Herman, M., Ho, L., Kreber, R., Honig, L.S., Ganetzky, B., Duff, K., Arancio, O., Small, S.A., 2008. Retromer deficiency observed in Alzheimer's disease causes hippocampal dysfunction, neurodegeneration, and Abeta accumulation. Proc. Natl. Acad. Sci. U. S. A. 105, 7327–7332.

Poewe, W., Mahlknecht, P., 2009. The clinical progression of Parkinson's disease. Parkinsonism Relat. Disord. 15 (Suppl. 4), S28–S32.

Press, B., Feng, Y., Hoflack, B., Wandinger-Ness, A., 1998. Mutant Rab7 causes the accumulation of cathepsin D and cation-independent mannose 6-phosphate receptor in an early endocytic compartment. J. Cell Biol. 140, 1075–1089.

Rojas, R., van Vlijmen, T., Mardones, G.A., Prabhu, Y., Rojas, A.L., Mohammed, S., Heck, A.J., Raposo, G., van der Sluijs, P., Bonifacino, J.S., 2008. Regulation of retromer recruitment to endosomes by sequential action of Rab5 and Rab7. J. Cell Biol. 183, 513–526.
Schneider, L., Zhang, J., 2010. Lysosomal function in macromolecular homeostasis and bioenergetics in Parkinson's disease. Mol. Neurodegener. 5, 14.
Seaman, M.N., 2004. Cargo-selective endosomal sorting for retrieval to the Golgi requires retromer. J. Cell Biol. 165, 111–122.
Seaman, M.N., Marcusson, E.G., Cereghino, J.L., Emr, S.D., 1997. Endosome to Golgi retrieval of the vacuolar protein sorting receptor, Vps10p, requires the function of the VPS29, VPS30, and VPS35 gene products. J. Cell Biol. 137, 79–92.
Seaman, M.N., Harbour, M.E., Tattersall, D., Read, E., Bright, N., 2009. Membrane recruitment of the cargo-selective retromer subcomplex is catalysed by the small GTPase Rab7 and inhibited by the Rab-GAP TBC1D5. J. Cell Sci. 122, 2371–2382.
Sevlever, D., Jiang, P., Yen, S.H., 2008. Cathepsin D is the main lysosomal enzyme involved in the degradation of alpha-synuclein and generation of its carboxy-terminally truncated species. Biochemistry 47, 9678–9687.
Singleton, A.B., Farrer, M.J., Bonifati, V., 2013. The genetics of Parkinson's disease: progress and therapeutic implications. Mov. Disord. 28, 14–23.
Small, S.A., Kent, K., Pierce, A., Leung, C., Kang, M.S., Okada, H., Honig, L., Vonsattel, J.P., Kim, T. W., 2005. Model-guided microarray implicates the retromer complex in Alzheimer's disease. Ann. Neurol. 58, 909–919.
Spillantini, M.G., Schmidt, M.L., Lee, V.M., Trojanowski, J.Q., Jakes, R., Goedert, M., 1997. Alpha-synuclein in Lewy bodies. Nature 388, 839–840.
Springer, W., Kahle, P.J., 2011. Regulation of PINK1-Parkin-mediated mitophagy. Autophagy 7, 266–278.
Sugeno, N., Takeda, A., Hasegawa, T., Kobayashi, M., Kikuchi, A., Mori, F., Wakabayashi, K., Itoyama, Y., 2008. Serine 129 phosphorylation of alpha-synuclein induces unfolded protein response-mediated cell death. J. Biol. Chem. 283, 23179–23188.
Sugeno, N., Hasegawa, T., Tanaka, N., Fukuda, M., Wakabayashi, K., Oshima, R., Konno, M., Miura, E., Kikuchi, A., Baba, T., Anan, T., Nakao, M., Geisler, S., Aoki, M., Takeda, A., 2014. K63-linked ubiquitination by E3 ubiquitin ligase Nedd4-1 facilitates endosomal sequestration of internalized alpha-synuclein. J. Biol. Chem. 289, 18137–18151.
Tardiff, D.F., Jui, N.T., Khurana, V., Tambe, M.A., Thompson, M.L., Chung, C.Y., Kamadurai, H.B., Kim, H.T., Lancaster, A.K., Caldwell, K.A., Caldwell, G.A., Rochet, J.C., Buchwald, S.L., Lindquist, S., 2013. Yeast reveal a "druggable" Rsp5/Nedd4 network that ameliorates alpha-synuclein toxicity in neurons. Science 342, 979–983.
Tofaris, G.K., 2012. Lysosome-dependent pathways as a unifying theme in Parkinson's disease. Mov. Disord. 27, 1364–1369.
Tofaris, G.K., Kim, H.T., Hourez, R., Jung, J.W., Kim, K.P., Goldberg, A.L., 2011. Ubiquitin ligase Nedd4 promotes alpha-synuclein degradation by the endosomal–lysosomal pathway. Proc. Natl. Acad. Sci. U. S. A. 108, 17004–17009.
Tsakiri, E.N., Iliaki, K.K., Hohn, A., Grimm, S., Papassideri, I.S., Grune, T., Trougakos, I.P., 2013. Diet-derived advanced glycation end products or lipofuscin disrupts proteostasis and reduces life span in Drosophila melanogaster. Free Radic. Biol. Med. 65c, 1155–1163.
Tsika, E., Glauser, L., Moser, R., Fiser, A., Daniel, G., Sheerin, U.M., Lees, A., Troncoso, J.C., Lewis, P.A., Bandopadhyay, R., Schneider, B.L., Moore, D.J., 2014. Parkinson's disease-linked mutations in VPS35 induce dopaminergic neurodegeneration. Hum. Mol. Genet. 23, 4621–4638.
Vilarino-Guell, C., Wider, C., Ross, O.A., Dachsel, J.C., Kachergus, J.M., Lincoln, S.J., Soto-Ortolaza, A.I., Cobb, S.A., Wilhoite, G.J., Bacon, J.A., Behrouz, B., Melrose, H.L., Hentati, E., Puschmann, A., Evans, D.M., Conibear, E., Wasserman, W.W., Aasly, J.O., Burkhard, P.R., Djaldetti, R., Ghika, J., Hentati, F., Krygowska-Wajs, A., Lynch, T., Melamed, E., Rajput, A., Rajput, A.H., Solida, A., Wu, R.M., Uitti, R.J., Wszolek, Z.K., Vingerhoets, F., Farrer, M.J., 2011. VPS35 mutations in Parkinson disease. Am. J. Hum. Genet. 89, 162–167.
Vilarino-Guell, C., Rajput, A., Milnerwood, A.J., Shah, B., Szu-Tu, C., Trinh, J., Yu, I., Encarnacion, M., Munsie, L.N., Tapia, L., Gustavsson, E.K., Chou, P., Tatarnikov, I., Evans, D.M., Pishotta, F.T., Volta, M., Beccano-Kelly, D., Thompson, C., Lin, M.K., Sherman, H.E., Han, H.J., Guenther, B.L., Wasserman, W.W., Bernard, V., Ross, C.J., Appel-Cresswell, S., Stoessl, A.J., Robinson, C.A., Dickson, D.W., Ross, O.A., Wszolek, Z.K., Aasly, J.O., Wu, R. M., Hentati, F., Gibson, R.A., McPherson, P.S., Girard, M., Rajput, M., Rajput, A.H., Farrer, M.J., 2014. DNAJC13 mutations in Parkinson disease. Hum. Mol. Genet. 23, 1794–1801.
Vogiatzi, T., Xilouri, M., Vekrellis, K., Stefanis, L., 2008. Wild type alpha-synuclein is degraded by chaperone-mediated autophagy and macroautophagy in neuronal cells. J. Biol. Chem. 283, 23542–23556.
Wales, P., Pinho, R., Lazaro, D.F., Outeiro, T.F., 2013. Limelight on alpha-synuclein: pathological and mechanistic implications in neurodegeneration. J. Parkinsons Dis. 3, 415–459.
Wen, L., Tang, F.L., Hong, Y., Luo, S.W., Wang, C.L., He, W., Shen, C., Jung, J.U., Xiong, F., Lee, D. H., Zhang, Q.G., Brann, D., Kim, T.W., Yan, R., Mei, L., Xiong, W.C., 2011. VPS35 haploinsufficiency increases Alzheimer's disease neuropathology. J. Cell Biol. 195, 765–779.
Yamaguchi, M., Hirose, F., Inoue, Y.H., Shiraki, M., Hayashi, Y., Nishi, Y., Matsukage, A., 1999. Ectopic expression of human p53 inhibits entry into S phase and induces apoptosis in the Drosophila eye imaginal disc. Oncogene 18, 6767–6775.
Zavodszky, E., Seaman, M.N., Moreau, K., Jimenez-Sanchez, M., Breusegem, S.Y., Harbour, M. E., Rubinsztein, D.C., 2014. Mutation in VPS35 associated with Parkinson's disease impairs WASH complex association and inhibits autophagy. Nat. Commun. 5, 3828.
Zhao, X., Nothwehr, S., Lara-Lemus, R., Zhang, B.Y., Peter, H., Arvan, P., 2007. Dominant-negative behavior of mammalian Vps35 in yeast requires a conserved PRLYL motif involved in retromer assembly. Traffic 8, 1829–1840.
Zimprich, A., Benet-Pages, A., Struhal, W., Graf, E., Eck, S.H., Offman, M.N., Haubenberger, D., Spielberger, S., Schulte, E.C., Lichtner, P., Rossle, S.C., Klopp, N., Wolf, E., Seppi, K., Pirker, W., Presslauer, S., Mollenhauer, B., Katzenschlager, R., Foki, T., Hotzy, C., Reinthaler, E., Harutyunyan, A., Kralovics, R., Peters, A., Zimprich, F., Brucke, T., Poewe, W., Auff, E., Trenkwalder, C., Rost, B., Ransmayr, G., Winkelmann, J., Meitinger, T., Strom, T.M., 2011. A mutation in VPS35, encoding a subunit of the retromer complex, causes late-onset Parkinson disease. Am. J. Hum. Genet. 89, 168–175.

Human Molecular Genetics, 2014, Vol. 23, No. 13 **3467–3480**
doi:10.1093/hmg/ddu055
Advance Access published on February 4, 2014

Identification of *ter94*, *Drosophila VCP*, as a strong modulator of motor neuron degeneration induced by knockdown of *Caz*, *Drosophila FUS*

Yumiko Azuma[1], Takahiko Tokuda[1,2,†,*], Mai Shimamura[3,4], Akane Kyotani[3,4], Hiroshi Sasayama[1], Tomokatsu Yoshida[1], Ikuko Mizuta[1], Toshiki Mizuno[1], Masanori Nakagawa[1], Nobuhiro Fujikake[5], Morio Ueyama[5], Yoshitaka Nagai[5] and Masamitsu Yamaguchi[3,4,†]

[1]Department of Neurology and [2]Department of Molecular Pathobiology of Brain Diseases, Graduate School of Medical Science, Kyoto Prefectural University of Medicine, 465 Kajii-cho, Kamigyo-ku, Kyoto 602-8566, Japan, [3]Department of Applied Biology and [4]Insect Biomedical Research Center, Kyoto Institute of Technology, Hashikami-cho, Matsugasaki, Sakyo-ku, Kyoto 606-8585, Japan and [5]Department of Degenerative Neurological Diseases, National Institute of Neuroscience, National Center of Neurology and Psychiatry, 4-1-1 Ogawa-Higashi, Kodaira, Tokyo 187-8502, Japan

Received October 3, 2013; Revised and Accepted January 31, 2014

In humans, mutations in the *fused in sarcoma* (*FUS*) gene have been identified in sporadic and familial forms of amyotrophic lateral sclerosis (ALS). *Cabeza* (*Caz*) is the *Drosophila* ortholog of human *FUS*. Previously, we established *Drosophila* models of ALS harboring *Caz*-knockdown. These flies develop locomotive deficits and anatomical defects in motoneurons (MNs) at neuromuscular junctions; these phenotypes indicate that loss of physiological FUS functions in the nucleus can cause MN degeneration similar to that seen in FUS-related ALS. Here, we aimed to explore molecules that affect these ALS-like phenotypes of our *Drosophila* models with eye-specific and neuron-specific *Caz*-knockdown. We examined several previously reported ALS-related genes and found genetic links between *Caz* and *ter94*, the *Drosophila* ortholog of human *Valosin-containing protein* (*VCP*). Genetic crossing the strongest loss-of-function allele of *ter94* with *Caz*-knockdown strongly enhanced the rough-eye phenotype and the MN-degeneration phenotype caused by *Caz*-knockdown. Conversely, the overexpression of wild-type *ter94* in the background of *Caz*-knockdown remarkably suppressed those phenotypes. Our data demonstrated that expression levels of *Drosophila* VCP ortholog dramatically modified the phenotypes caused by *Caz*-knockdown in either direction, exacerbation or remission. Our results indicate that therapeutic agents that up-regulate the function of human VCP could modify the pathogenic processes that lead to the degeneration of MNs in ALS.

INTRODUCTION

Amyotrophic lateral sclerosis (ALS) is a devastating neurodegenerative disease that is characterized by degeneration of motoneurons (MNs); this degeneration leads to progressive muscle weakness and eventually fatal paralysis typically within 1–5 years after disease onset (1). Frontotemporal lobar degeneration (FTLD) is a dementia syndrome with clinically diverse phenotypes that include behavioral changes, semantic dementia and progressive non-fluent aphasia (2). It is well established that ALS and FTLD form a clinical disease continuum (3,4). Up to 15% of ALS patients meet the clinical criteria of FTLD and 30–50% has subtle cognitive deficits (5); likewise, up to 15% of FTLD patients meet the clinical criteria for ALS and up to one-third have at least minor MN dysfunction (5).

* To whom correspondence should be addressed at: Department of Molecular Pathobiology of Brain Diseases, Graduate School of Medical Science, Kyoto Prefectural University of Medicine, 465 Kajii-cho, Kamigyo-ku, Kyoto 602-8566, Japan. Tel: +81 752515793; Fax: +81 752118645; Email: ttokuda@koto.kpu-m.ac.jp
†Co-corresponding authors.

A substantial number of proteins linked to ALS are directly or indirectly involved in RNA processing (6). Mutations in genes encoding two such RNA-binding proteins—transactive response DNA binding protein 43 kDa (TDP-43, gene *TARDBP*) and fused in sarcoma (FUS, gene *FUS*)—have been identified as major genetic causes in both familial and sporadic ALS (2,7–15). TDP-43 and FUS are RNA-binding proteins implicated in multiple aspects of RNA metabolism including transcriptional regulation, mRNA splicing and shuttling of mRNAs between the nucleus and the cytoplasm (16,17).

There is a single *Drosophila* ortholog each for human FUS and TDP-43 named Cabeza (Caz) and TBPH, respectively. Reportedly, *Drosophila* lacking TBPH presented deficient locomotive behaviors, reduced life span and anatomical defects at neuromuscular junctions (NMJs); these phenotypes indicate that a loss of TDP-43 nuclear functions could be a causative factor for the neurodegeneration observed in patients with ALS/FTLD (18). Recently, we reported a fly model of ALS based on neuron-specific Caz-knockdown, which developed locomotive deficits and anatomical defects in MNs at NMJs; these findings demonstrate that loss of physiological functions of FUS in the nucleus could cause the neurodegeneration in FUS-related ALS/FTLD (19). There is substantial evidence that depletion of FUS in zebrafish or in *Drosophila* also causes MN degeneration that can be rescued by the respective wild-type but not mutant *FUS* (20,21). These findings suggest that FUS is important for the survival of MNs and that a "loss-of-function" mechanism could be the fundamental pathogenic mechanism causing FUS-related ALS/FTLD.

Using our established fly model of FUS-ALS induced by *Caz*-knockdown, we aimed to explore molecules that affect phenotypes presented by the model. Specifically, we intended to elucidate the molecular mechanisms leading to neuronal dysfunction in FUS-related ALS/FTLD in order to facilitate the development of disease-modifying therapies, which are eagerly desired for the treatment of those relentless neurodegenerative diseases. Initially, we focused on determining whether or not several ALS-related genes affect the phenotypes presented by our fly models, and we found a genetic link between *Caz* and *ter94*, which is the *Drosophila* ortholog of human *Valosin-containing protein* (*VCP*).

VCP is a member of the AAA (ATPase associated with a variety of cellular activities) family of proteins, which are implicated in a large variety of biological functions including the regulation of ubiquitin-dependent protein degradation, control of membrane fusion and of dynamics of subcellular components, vesicle-mediated transport and nucleocytoplasmic shuttling (22–24). Association of *VCP* mutations with human disease was first identified in patients with IBMPFD (inclusion body myopathy with early-onset Paget disease and frontotemporal dementia) (25) and more recently in those with ALS (26). There is a single ortholog of human *VCP* in *Drosophila,* named *ter94*, which is predicted to share ~83% amino acid sequence identity with human VCP.

Here, we found that genetic crossing the strongest loss-of-function allele of *ter94* with *Caz*-knockdown severely enhanced the *Caz*-knockdown phenotypes in flies; it severely exacerbated locomotive disabilities and the degeneration of MNs induced by neuron-specific *Caz*-knockdown. Conversely, the overexpression of *ter94* rescued those phenotypes.

RESULTS

Knockdown of *Caz* in eye imaginal discs induces morphologically aberrant rough eyes

To investigate the molecular mechanisms of FUS-related neurodegeneration, we have already generated *Caz*-knockdown fly models of ALS by using the highly versatile GAL4/UAS-targeted expression system (19). To eliminate the possibility of off-target effects, we generated 11 independent transgenic fly lines and obtained one fly line from the Vienna *Drosophila* RNAi center (VDRC; Table 1); *Caz* double-stranded RNA (dsRNA; inverted repeats, IRs) targeted to the different region of the *Caz* mRNA is expressed in those fly lines as described in our previous study (19). The RNAi of the fly lines we generated (responder controls) was targeted to the region corresponding to residues 1–167 (four lines, UAS-*Caz*-IR_{1-167}) and 180–346 (seven

Table 1. Associated phenotypes of fly strains carrying UAS-Caz-IR crossed with different GAL4 driver strains

	Transgene strain	Chromosome linkage	Act5C-GAL4> 28°C	Act5C-GAL4> 25°C	GMR-GAL4>	elav>GAL4
UAS-*Caz*-IR_{1-167}	3	III	Lethal	Lethal		
	4	III	Lethal	NE	Mild rough eye	ND
	11	II	Lethal	NE	Mild rough eye	ND
	21	III	Lethal	NE	Mild rough eye	ND
UAS-*Caz*-$IR_{180-346}$	11	II	NE	NE	Mild rough eye	NE
	12	II	NE	NE	Mild rough eye	NE
	17	II	NE	NE	Mild rough eye	ND
	22	III	NE	ND	Mild rough eye	NE
	24	III	NE	NE	ND	NE
	32	III	NE	ND	Mild rough eye	ND
	33	III	NE	NE	Mild rough eye	ND
UAS-*Caz*-$IR_{363-399}$		II	NE	ND	Mild rough eye	LD

We used two independent Caz-RNAi constructs, UAS-*Caz*-IR_{1-167} and UAS-*Caz*-$IR_{180-346}$, to generate 11 independent transgenic fly lines. UAS-*Caz*-$IR_{363-399}$ was obtained from VDRC. To drive the expression of *Caz* dsRNA in the whole body of the flies, or specifically in the eye imaginal discs or neuronal tissues, we cross UAS-*Caz*-IR flies with *Act5C-GAL4*, *GMR-GAL4* or *elav-GAL4* flies, respectively. Phenotypes associated with the resultant genotypes are summarized. Each transgenic strain shows a consistent phenotype. NE, no effect; ND, not determined; LD, locomotive dysfunction.

lines, UAS-*Caz*-IR$_{180-346}$) of *Drosophila* Caz, respectively. The RNAi of the fly strain obtained from the VDRC (w; UAS-*Caz*-IR$_{363-399}$; +) was targeted to the region corresponding to residues 363–399 of *Drosophila* Caz (UAS-*Caz*-IR$_{363-399}$).

Reportedly, *Caz* mRNA and Caz protein are enriched in the central nervous system (CNS), and Caz protein is present in eye imaginal discs (27). To efficiently screen for genes that affect the phenotypes caused by *Caz*-knockdown, we generated model flies with eye-specific *Caz*-knockdown. Specific knockdown of *Caz* in eye imaginal discs was achieved by crossing the transgenic flies carrying a UAS-*Caz*-IR, in which *Caz* dsRNA is expressed, with *GMR-GAL4* driver lines (*GMR-GAL4*; UAS-*Caz*-IR/+; +). Phenotypes of those model flies are easily characterized by abnormal rough eye morphology; scanning electron microscope (SEM) images showed fusion of ommatidia and loss of mechanosensory bristles (Fig. 1). Phenotypes of those fly lines carrying each UAS-*Caz*-IR crossed with the *GMR-GAL4* driver strain are summarized in Table 1. Flies carrying *GMR-GAL4*; +; + alone exhibited apparently normal eye morphology (Fig. 1A; *GMR*). Flies carrying *GMR-GAL4*; UAS-*Caz*-IR$_{1-167}$/+; + (GMR>UAS-*Caz*-IR$_{1-167}$) and those carrying *GMR-GAL4*; UAS-*Caz*-IR$_{363-399}$/+; + (GMR> UAS-*Caz*-IR$_{363-399}$) showed essentially the same rough-eye phenotype (Fig. 1B and C). These results demonstrated that the rough-eye phenotype observed in *Caz*-knockdown flies was not due to a possible insertional mutation or off-target effect, but rather to reduced Caz protein levels. Throughout the following studies, we used fly strains carrying UAS-*Caz*-IR$_{363-399}$, and UAS-*Caz*-IR hereafter refers to this fly strain.

Loss-of-function mutations and overexpression of *ter94* conversely modified the compound eye degeneration induced by *Caz*-knockdown

To examine a genetic interaction between *Caz* and ALS-causing genes, we first crossed eye-specific *Caz*-knockdown flies with several fly lines carrying different mutations in various ALS-causing genes, and their progeny were screened for eye phenotypes. From these screens, we detected a genetic interaction between *Caz* and *ter94*, the *Drosophila* ortholog of human *VCP*. We crossed *Caz*-knockdown flies with ethyl methanesulfonate-induced *ter94* mutations, $ter94^{K15502}$ and $ter94^{03775}$. The phenotypic characterization of two P-element alleles of *ter94* mutations was described previously (28). According to this report, female germ-line clones of a strong loss-of-function allele of *ter94*, $ter94^{K15502}$, do not produce germaria or egg chambers, and female germ-line clones of another slightly less strong loss-of-function allele of *ter94*, $ter94^{03775}$, formed germalia which give rise to stage 6 or 7 egg chambers before degeneration occurs (28). From these findings, we used the $ter94^{K15502}$ mutation as a strongest loss-of-function allele and the $ter94^{03775}$ mutation as a strong loss-of-function allele. The strongest ($ter94^{K15502}$) and strong ($ter94^{03775}$) loss-of-function mutations in the heterozygous states remarkably enhanced the rough-eye phenotype induced by eye-specific *Caz*-knockdown GMR>UAS-*Caz*-IR$_{363-399}$/ $ter94^{K15502}$ (Fig. 1D) and GMR>UAS-*Caz*-IR$_{363-399}$/ $ter94^{03775}$ (Fig. 1E), respectively. The progeny of eye-specific *Caz*-knockdown flies became lethal at the pupal stage when crossed with *ter94*-knockdown or a chromosomal deficiency line: *Df (2R) X1* lacking the genomic region 46C2-47A01 that contains *ter94*. These results indicate that loss-of-function mutations of *ter94* act as dominant enhancers of the *Caz*-knockdown-induced rough-eye phenotype. Conversely, the overexpression of wild-type *ter94* (GMR>UAS-*Caz*-IR$_{363-399}$/ UAS-*ter94*) obviously suppressed the rough-eye phenotype induced by eye-specific *Caz*-knockdown (Fig. 1G) based on a comparison with the responder control of UAS-*ter94* flies (GMR>UAS-*Caz*-IR$_{363-399}$/UAS-*GFP*) (Fig. 1F).

Loss-of-function mutation and overexpression of *ter94* had opposite effects on nuclear Caz signals in the larval CNS

We demonstrated in our previous paper that *Drosophila* Caz was strongly expressed in the CNS of third instar larvae and localized in the nucleus (19). Therefore, we investigated whether neuron-specific *Caz*-knockdown changed the expression or subcellular localization of Caz or both; specifically, we crossed fly lines carrying UAS-*Caz*-IR with *elav-GAL4* driver lines. To monitor Caz expression and localization, we immunostained brain-ventral ganglia complexes (BVGCs) of third instar larvae with anti-Caz antibody, which was developed previously (19), and quantified the immunofluorescent signals. The BVGCs of the control larvae, which carried w; +; *elav-GAL4*/+ (*elav*/+), exhibited ubiquitous signals of endogenous Caz (Fig. 2, a driver control, A1), but the signal intensity of endogenous Caz in the BVGCs was remarkably reduced in neuron-specific *Caz*-knockdown larvae carrying UAS-*Caz*-IR/+; *elav-GAL4*/+ (Fig. 2, elav>UAS-*Caz*-IR, C1). In driver control larvae, anti-Caz immunoreactivity was evident in the nucleus of the neuronal cells, but it did not colocalize with actin filaments stained with phalloidin (Fig. 2, B1, B2, B1+B2) or with chromosomes stained with diamino-2-phenylidole (DAPI; Fig. 2, B1, B3, B1+B3). These findings indicated that Caz must localize in the nucleoplasm. The intensity of nuclear Caz signals was significantly reduced in the BVGCs of neuron-specific *Caz*-knockdown larvae carrying elav>UAS-*Caz*-IR [intensity units = 8.89 (arbitrary units), measured in Fig. 2, D1] compared with that of driver control larvae (intensity units = 31.5, measured in Fig. 2, B1; $P < 0.001$, Fig. 2G).

Next, we examined the effects of ter94 on neuron-specific *Caz*-knockdown with regard to Caz levels and localization. First, we examined Caz expression and localization in larvae carrying a heterozygous loss-of-function *ter94* mutation and neuron-specific *Caz*-knockdown constructs. Larvae carrying the strongest loss-of-function allele of *ter94* and neuron-specific *Caz*-knockdown, UAS-*Caz*-IR/ $ter94^{K15502}$; *elav-GAL4*/+ (Fig. 2, elav>UAS-*Caz*-IR/$ter94^{K15502}$, E1) exhibited remarkably reduced Caz signals in the BVGCs when compared with UAS-*Caz*-IR/+; *elav-GAL4*/+ larvae. The intensity of nuclear Caz signal was significantly reduced in these larvae carrying elav>UAS-*Caz*-IR/$ter94^{K15502}$ (intensity units = 6.68, measured in Fig. 2, F1), even compared with that of the larvae carrying elav>UAS-*Caz*-IR (Fig. 2, D1) ($P < 0.05$, Fig. 2G). These results indicated that neuron-specific *Caz*-knockdown significantly reduced nuclear Caz expression, and this reduction was enhanced by genetic crossing with the strongest loss-of-function allele of *ter94*.

Conversely, compared with the Caz signals in BVGCs of larvae carrying UAS-*Caz*-IR/UAS-*GFP*; *elav-GAL4*/+ (Fig. 3, elav>UAS-*Caz*-IR/UAS-*GFP*, A1), Caz signals in

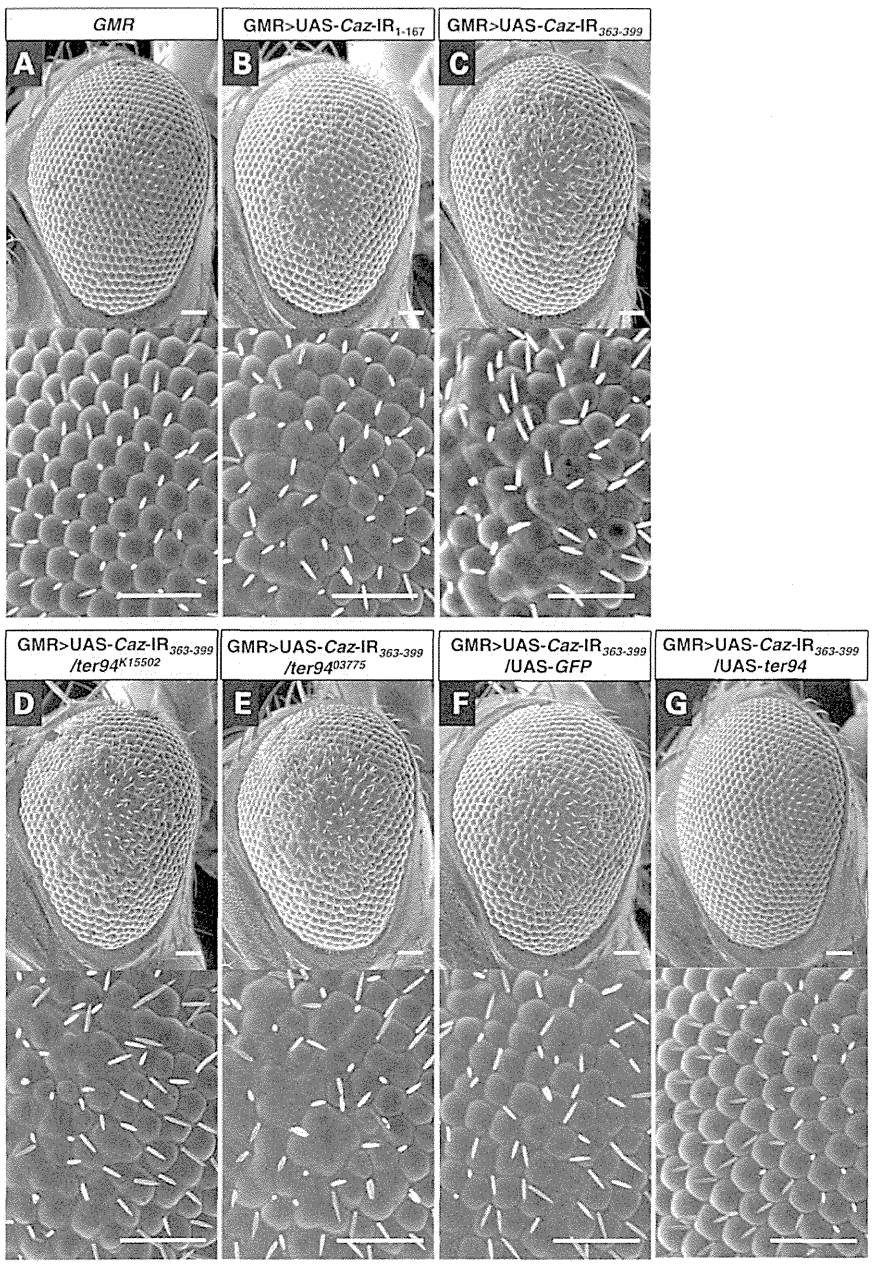

Figure 1. The rough-eye phenotype induced by *Caz*-knockdown is modified by genetic changes in *ter94*. Each panel shows a scanning electron micrograph of the compound eye of a 3-day-old adult fly. Each lower panel is a higher magnification image of the corresponding upper panel. Specific knockdown of *Caz* in eye imaginal discs was achieved by crossing the transgenic flies that carried UAS-*Caz*-IR with the *GMR-GAL4* driver. (**A**) The eyes of a control fly carrying *GMR-GAL4*; +; + (*GMR*) exhibit apparently normal eye morphology having an organized ommatidial architecture. (**B** and **C**) Adult eyes from two independent fly lines with eye-specific *Caz*-knockdown. Flies from line with UAS-*Caz*-IR1–167 (strain 4, Table 1) or from the line with UAS-*Caz*-IR363–399 were crossed with flies from the *GMR-GAL4* driver strain. Resultant flies carrying GMR>UAS-*Caz*-IR1–167 (B) or GMR>UAS-*Caz*-IR363–399 (C) have essentially the same rough-eye phenotype and exhibit ommatidial degeneration. (**D** and **E**) Adult eyes from two independent fly lines; each line has eye-specific *Caz*-knockdown and a distinct loss-of-function mutation in *ter94*. The eye-specific *Caz*-knockdown fly line (GMR>UAS-*Caz*-IR363–399/UAS-*Caz*-IR363–399) was crossed with flies carrying the strongest ($ter94^{K15502}$) or a strong ($ter94^{03775}$) loss-of-function *ter94* mutation. The resultant flies carrying GMR>UAS-*Caz*-IR363–399/$ter94^{K15502}$ (D) or GMR>UAS-*Caz*-IR363–399/$ter94^{03775}$ (E) show rough-eye phenotypes that is enhanced relative to that observed in flies with GMR>UAS-*Caz*-IR363–399 alone (C). Adult eyes from fly lines resulting from crosses of eye-specific *Caz*-knockdown flies with UAS-*GFP* (GMR>UAS-*Caz*-IR363–399/UAS-*GFP*, a responder control, **F**) or UAS-*ter94* (GMR>UAS-*Caz*-IR363–399/UAS-*ter94*, **G**). The rough-eye phenotype induced by eye-specific *Caz*-knockdown is obviously less severe in the presence of UAS-*ter94* (G) than in the presence of UAS-*GFP* (F). Posterior is to the right, and dorsal is to the top. The flies were developed at 28°C. Scale bars indicate 50 μm.

BVGCs were remarkably stronger in larvae carrying UAS-*Caz*-IR/ UAS-*ter94*; *elav-GAL4*/+, in which wild-type *ter94* was overexpressed under the *Caz*-knockdown background (Fig. 3, elav>UAS-*Caz*-IR/UAS-*ter94*, C1). Quantification of the Caz signal revealed that the intensity of nuclear Caz signal was 3.69-fold higher in elav>UAS-*Caz*-IR/UAS-*ter94* larvae (intensity units = 23.5, measured in Fig. 3, D1) than in elav> UAS-*Caz*-IR/UAS-*GFP* larvae (intensity units = 6.36, measured in Fig. 3, B1; $P < 0.001$, Fig. 3E). These results indicated that overexpression of wild-type *ter94* restored the reduced Caz signal in the nucleus induced by neuron-specific *Caz*-knockdown. Taken together, our presented results suggest that ter94 levels could enhance or rescue the Caz-knockdown phenotype.

To clarify whether or not altered ter94 protein levels affect the knock-down machinery, we carried out immunoblot analyses of CNS extracts of third instar larvae carrying *elav*/+, elav>UAS-*Caz*-IR, elav>UAS-*Caz*-IR/*ter94* ^{K15502}, elav>UAS-*Caz*-IR/UAS-*GFP* and elav>UAS-*Caz*-IR/UAS-*ter94*. A single major band with an apparent molecular weight of 45 kDa was detected on immunoblots of all the flies using the anti-Caz antibody (Supplementary Material, Fig. S1A). The intensity of this Caz protein band was apparently reduced in larvae carrying elav>UAS-*Caz*-IR compared with its intensity in larvae carrying *elav*/+ (Supplementary Material, Fig. S1A and B). We then found that there was no apparent difference in Caz protein levels of CNS extracts either between the larvae carrying elav>UAS-*Caz*-IR and elav>UAS-*Caz*-IR/ *ter94*^{K15502} or between the larvae carrying elav>UAS-*Caz*-IR/UAS-*GFP* and elav>UAS-*Caz*-IR/UAS-*ter94* (Supplementary Material, Fig. S1A and B). These results suggest that ter94 levels do not affect the Caz protein level on *Caz*-knockdown larvae, but indeed decrease or restore nuclear Caz protein levels in *Caz*-knockdown larvae.

Effects of a loss-of-function mutation and of overexpression of *ter94* on the mobility defects caused by neuron-specific *Caz*-knockdown

Because ALS is an age-related motor neuron disease, we examined the effect of neuron-specific *Caz*-knockdown on the locomotive function of adult flies of different ages by using a well-established climbing assay (29). We also examined the effects of loss-of-function or overexpression of *ter94* on changes in climbing ability caused by neuron-specific *Caz*-knockdown. All the fly strains showed an age-dependent decline in the climbing ability (Fig. 4). Neuron-specific *Caz*-knockdown flies carrying elav>UAS-*Caz*-IR exhibited a significantly decreased climbing ability at the following days of age; day 7, −10.4%; and day 21, −16.8%, $P < 0.001$; day 14, −10.6%, $P < 0.01$; day 28, −14.7%, $P < 0.05$ (Fig. 4A, gray columns). Flies carrying the strongest loss-of-function allele of *ter94* and neuron-specific *Caz*-knockdown (elav>UAS-*Caz*-IR/*ter94*^{K15502}) had significantly worse locomotive ability than did flies with neuron-specific *Caz*-knockdown alone (elav>UAS-*Caz*-IR) for every age examined (day 3, −14.0%; day 7, −19.5%; day 14, −35.2%; day 21, −49.7%; day 28, −63%; $P < 0.001$, Fig. 4A, black columns). Conversely, flies that overexpressed wild-type *ter94* in the background of neuron-specific *Caz*-knockdown (elav>UAS-*Caz*-IR/UAS-*ter94*) had significantly better climbing ability than did control flies with neuron-specific *Caz*-knockdown (elav>UAS-*Caz*-IR/UAS-*GFP*) until day 14 (day 3, +24.8%; day 14, +21.8%, $P < 0.001$; day 7, +15.5%, $P < 0.01$; Fig. 4B, black columns), but not after that (day 21, not significant, $P = 0.98$; day 28, reduced climbing ability, −37.4%, $P < 0.01$; Fig. 4B, black columns). There were no significant differences in climbing abilities among *elav*/+ (a driver control), UAS-*Caz*-IR/+ (a responder control) and *ter94* ^{K15502}/+ flies in each day after exclusion that was monitored until 14 days (Supplementary Material, Fig. S2). Flies carrying elav>UAS-*Caz*-IR/UAS-*GFP* exhibited a significantly decreased climbing ability for every age examined (day 3, −32.8%; day 7, −23.8%; day14, −26.1%; day 21, −42.4%; day 28, −47.9%, $P < 0.001$; Fig. 4B, gray columns) compared with those carrying *elav*/+ (Fig. 4B, white columns). Until day 3, the climbing ability of flies carrying elav>UAS-*Caz*-IR/UAS-*ter94* was recovered almost as well as that of flies carrying *elav*/+. However, that of flies carrying elav>UAS-*Caz*-IR/UAS-*ter94* was not fully recovered, and significantly less than that of those carrying *elav*/+ after day 3 at the following days of age; day 7, −12.8%; day 21, −42.4%; day 28, −27.8%, $P < 0.001$; day 14, −10.0%, $P < 0.01$ (Fig. 4B, black columns) compared with those carrying *elav*/+ (Fig. 4B, white columns). Together, our data demonstrate that neuron-specific *Caz*-knockdown leads to a severe progressive locomotive defect in adult flies, and that overexpression of wild-type *ter94* could rescue the locomotive defect until certain fly ages, whereas loss of *ter94* function significantly exacerbated this *Caz*-knockdown defect throughout the adult life span of these flies. We next examined the fly life span of the fly models with neuron-specific *Caz*-knockdown and genetically modified *ter94*. There were no significant differences in life spans among the control flies carrying *elav*/+ (the average life span = 50.9 days, $n = 151$), neuron-specific *Caz*-knockdown flies carrying elav>UAS-*Caz*-IR (48.3 days, $n = 123$), and flies carrying the strongest loss-of-function allele of *ter94* and neuron-specific *Caz*-knockdown (elav> UAS-*Caz*-IR/*ter94*^{K15502}, 47.5 days, $n = 120$) (Supplementary Material, Fig. S3A). Similarly, there were no significant differences in life spans between neuron-specific *Caz*-knockdown flies carrying elav>UAS-*Caz*-IR/UAS-*GFP* (responder control, the average life span = 44.8 days, $n = 140$) and those carrying *ter94* overexpression in the background of neuron-specific *Caz*-knockdown, elav>UAS-*Caz*-IR/UAS-*ter94* (41.1 days, $n = 140$) (Supplementary Material, Fig. S3B). In our Caz-knockdown fly models, the expression of Caz protein was decreased to 40–60% in the CNS, but their life spans were not reduced (19). These results suggest that the substantial expression of Caz in neuronal tissues, even though it is not fully expressed, could sufficiently keep their life spans within normal range.

The effects of loss-of-function mutation and overexpression of *ter94* on the morphology of MN presynaptic terminals in the NMJs of neuron-specific *Caz*-knockdown flies

Based on the finding that our *Caz*-knockdown flies showed motor deficits in the climbing assay (19) and the fact that *FUS*, the human ortholog of *Caz*, is involved in ALS that impairs motor neurons, we analyzed the morphology of MN presynaptic

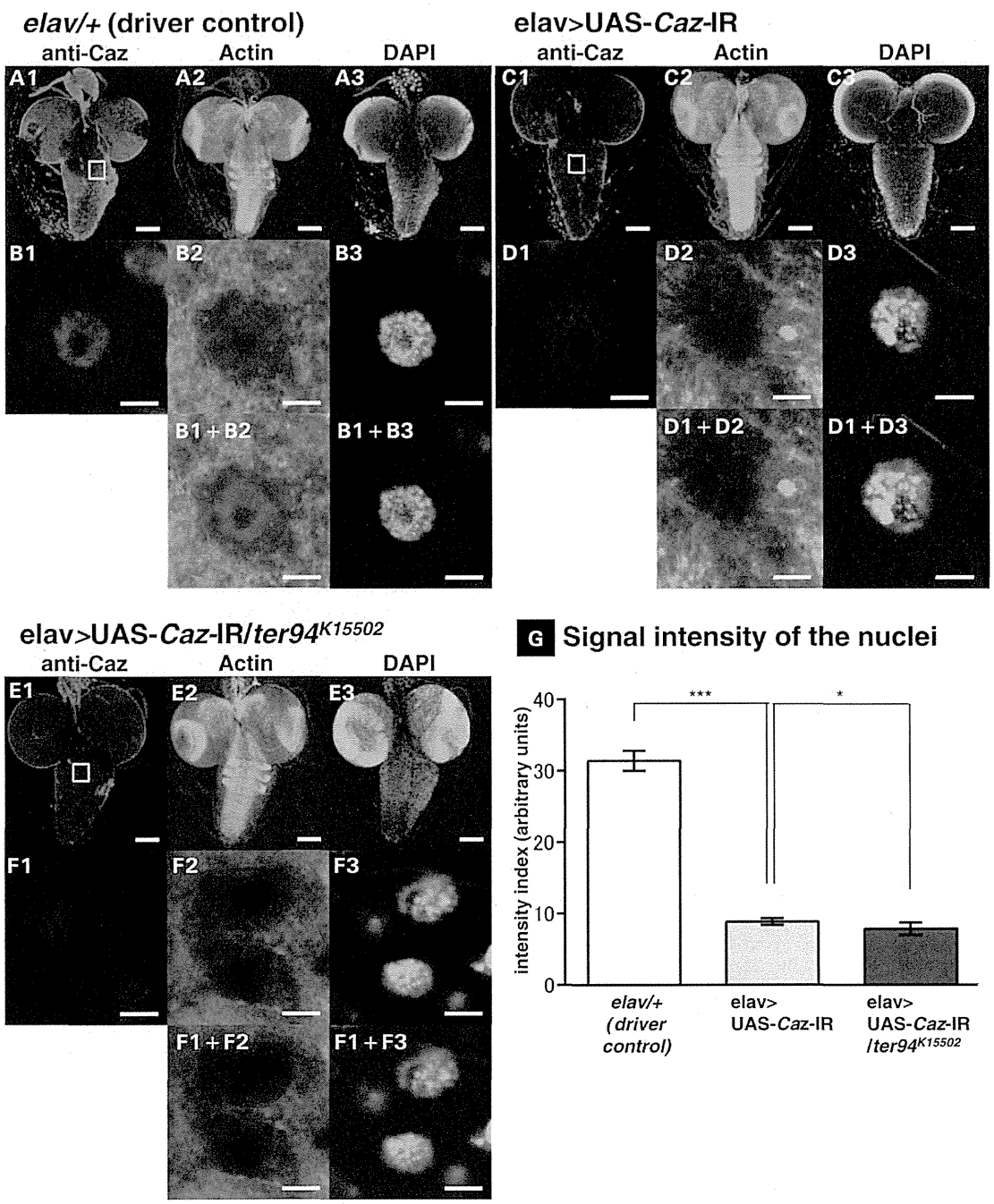

Figure 2. Neuron-specific *Caz*-knockdown reduces Caz signal in nuclei within larval CNS, and this reduction is significantly exacerbated by a loss-of-function *ter94* mutation. **(A)**–**(F)** are representative images of corresponding genotypes. (A1)–(A3) are immunofluorescent images of larval CNS, which comprises BVGC, taken from a driver control larva carrying *elav/+*. (C1)–(C3) are the BVGCs of a *Caz*-knockdown larva carrying UAS-*Caz*-IR. (E1)–(E3) are the BVGCs of a larva co-expressed with $ter94^{K15502}$ in the background of *Caz*-knockdown carrying elav>UAS-*Caz*-IR/$ter94^{K15502}$. (B1)–(B3), (D1)–(D3) and (F1)–(F3) are higher magnification images of the boxed area in (A1), (C1) and (E1), respectively. (B1+B2), (B1+B3), (D1+D2), (D1+D3), (F1+F2) and (F1+F3) are merged images. The indirect immunofluorescence in A1, B1, C1, D1, E1 and F1 is signal from the polyclonal anti-Caz antibody. The fluorescence in A2, B2, C2, D2, E2 and F2 is from phalloidin, which labels actin; the fluorescence in A3, B3, C3, D3, E3 and F3 is from DAPI, which labels DNA. The BVGC of driver control larvae carrying *elav/+* show ubiquitous signals from endogenous Caz (A1), but the signal intensity from endogenous Caz in the BVGC is remarkably reduced in larvae carrying elav>UAS-*Caz*-IR (C1). Anti-Caz antibody immunoreactivity is evident in the nuclei of neuronal cells (B1) and does not colocalize with phalloidin-stained actin filaments (B2, B1+B2). Caz does not colocalize with DAPI (B3, B1+B3). The intensity of nuclear Caz signal is significantly reduced in the BVGCs of larvae carrying

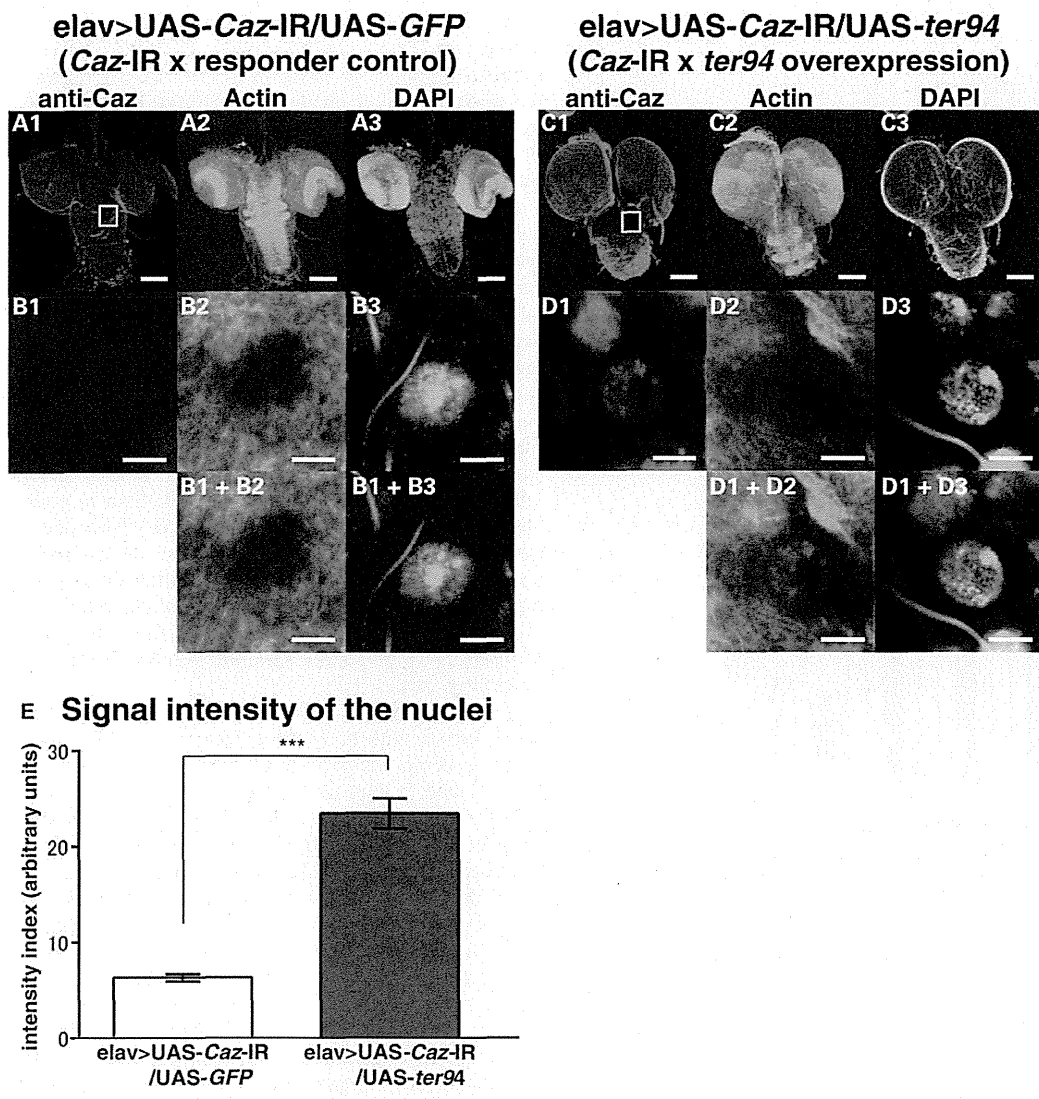

Figure 3. Overexpression of wild-type *ter94* restores Caz signal in nuclei in the CNS of larvae with neuron-specific *Caz*-knockdown. (**A**)–(**D**) are representative images of corresponding genotypes. (A1)–(A3) are the BVGCs of a *Caz*-knockdown larva carrying elav>UAS-*Caz*-IR/UAS-*GFP*. (C1)–(C3) are the BVGCs of a larva that overexpressed wild-type *ter94* in the background of *Caz*-knockdown carrying elav>UAS-*Caz*-IR/UAS-*ter94*. (B1)–(B3) and (D1)–(D3) are higher magnification images of the boxed area in A1 and C1, respectively. (B1+B2), (B1+B3), (D1+D2) and (D1+D3) are merged images. The indirect immunofluorescence in A1, B1, C1 and D1 is the signal from the polyclonal anti-Caz antibody. The fluorescence in A2, B2, C2 and D2 and that in A3, B3, C3 and D3 are from phalloidin and DAPI, respectively. (**E**) shows the mean (± SE) of the intensity of the nuclear Caz signal in the BVGC tissues from the third instar larvae as fluorescence emission in arbitrary units. Columns and horizontal bars show the mean and SE of 15 nuclei, respectively. $^{***}P < 0.001$. Compared with the Caz signals in the BVGCs of the larvae carrying elav>UAS-*Caz*-IR/UAS-*GFP* (A1), Caz signals are remarkably stronger in the BVGCs of the larvae carrying elav>UAS-*Caz*-IR/UAS-*ter94* (C1). The intensity of the nuclear Caz signal is significantly higher in these larvae due to the overexpression of *ter94* (D1) than in the larvae carrying elav>UAS-*Caz*-IR/UAS-*GFP* (B1) ($P < 0.001$, E). The scale bars indicate 100 μm (A1–A3 and C1–C3) and 5 μm (B1–B3 and D1–D3).

elav>UAS-*Caz*-IR (D1) compared with that of driver control larvae (B1) ($P < 0.001$, G). The larvae carrying the strongest loss-of-function allele of *ter94* and neuron-specific *Caz*-knockdown (elav>UAS-*Caz*-IR/*ter94*^{K15502}) (E1) also show remarkably reduced Caz signals in the BVGCs. The intensity of the nuclear Caz signal is significantly reduced in these larvae with the strongest loss-of-function allele of *ter94* and *Caz*-knockdown (F1), even compared with that of the *Caz*-knockdown larvae (D1) ($P < 0.05$, **G**). The scale bars indicate 100 μm (A1–A3, C1–C3 and E1–E3) and 5 μm (B1–B3, D1–D3 and F1–F3). (G) This graph plots the mean (± SE) of the intensity of the nuclear Caz signal in BVGCs from third instar larvae as fluorescence emission in arbitrary units with respect to the genotype; Columns and horizontal bars show the mean and SE of 15 nuclei, respectively. $^{***}P < 0.001$, $^{*}P < 0.05$.

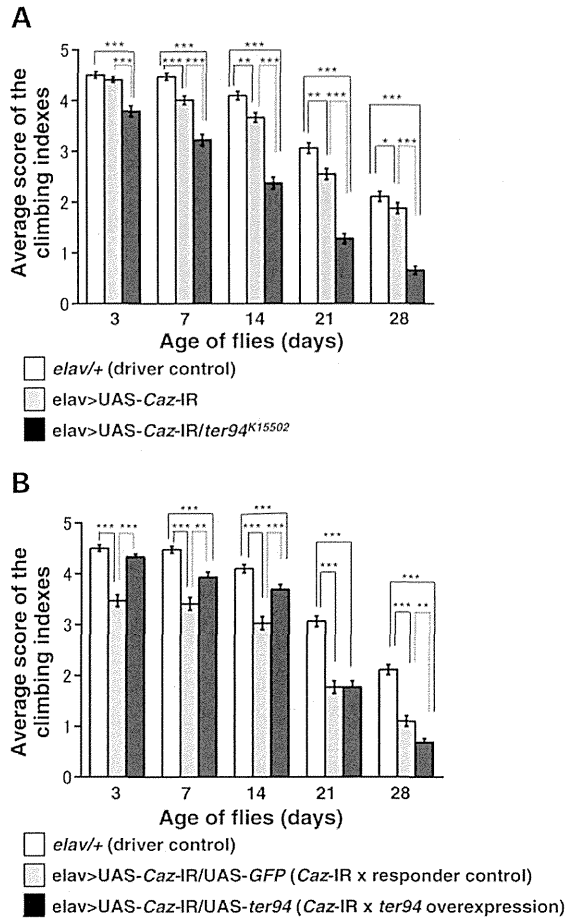

Figure 4. A loss-of-function *ter94* mutation and wild-type *ter94* overexpression have opposite effects on the climbing ability of neuron-specific *Caz*-knockdown flies. (**A**) The locomotive ability of driver control flies, which carrying *elav/+* ($n = 366$, white columns), is significantly better than that of neuron-specific *Caz*-knockdown flies, which carrying elav>UAS-*Caz*-IR ($n = 296$, gray columns) for every age examined other than day 3. On each day after eclosion that was monitored, adult flies carrying elav>UAS-*Caz*-IR/*ter94*^{K15502} ($n = 210$, black columns) exhibited significantly worse climbing ability than flies carrying neuron-specific *Caz*-knockdown alone. (**B**) Conversely, adult flies carrying elav>UAS-*Caz*-IR/UAS-*ter94* ($n = 215$, black columns) have significantly better climbing ability than flies carrying elav>UAS-*Caz*-IR/UAS-*GFP* ($n = 190$, gray columns) on days 3, 7 and 14, but not after day 14. The climbing ability of flies carrying *elav/+* ($n = 366$, white columns) is significantly better than those carrying elav>UAS-*Caz*-IR/UAS-*GFP* for every age examined, same as those in (A). Until day 3, the climbing ability of flies carrying elav>UAS-*Caz*-IR/UAS-*ter94* is recovered almost as well as that of flies carrying *elav/+*. However, that of the flies carrying elav>UAS-*Caz*-IR/UAS-*ter94* is significantly less than that of flies carrying *elav/+* after day 3. Columns and horizontal bars show the mean and SE of the measurements, respectively. $^{***}P < 0.001$, $^{**}P < 0.01$ and $^{*}P < 0.05$.

terminals at NMJs in *Caz*-knockdown flies. Abnormal NMJ morphology and behavioral defects have been implicated in many *Drosophila* models of neurodegenerative diseases that involve motor disturbances such as spinal muscular atrophy and tauopathies (30,31). Because most MNs of the adult fly originate from larval MNs, we examined the NMJ structure in the larvae from *Caz*-knockdown strains. Previously, we demonstrated that neuron-specific *Caz*-knockdown shortened terminal branches of larval MNs (19). To clarify the effects of the *ter94* mutation on the morphology of MN terminals, we examined the NMJ structure of our *Caz*-knockdown flies with or without *ter94* mutation and with or without wild-type *ter94* overexpression.

Compared with the total length of synaptic branches of MNs in driver control larvae carrying *elav/+* (94.4 ± 8.0 μm, Fig. 5A), which was significantly decreased in neuron-specific *Caz*-knockdown larvae carrying elav>UAS-*Caz*-IR (53.8 ± 6.0 μm, Fig. 5B; $P < 0.001$, Fig. 5D). Furthermore, this decreased branch length caused by neuron-specific *Caz*-knockdown was significantly enhanced by genetic crossing with the strongest loss-of-function allele of *ter94* (elav>UAS-*Caz*-IR/*ter94*^{K15502}, 39.5 ± 1.7 μm, Fig. 5C; $P = 0.035$, Fig. 5D). The average number of synaptic boutons per MN was also significantly smaller in neuron-specific *Caz*-knockdown larvae (9.7 ± 0.5, Fig. 5B) than in control larvae (14.7 ± 1.0, Fig. 5A; $P < 0.001$, Fig. 5E). This decrease in the number of synaptic boutons in the neuron-specific *Caz*-knockdown larvae was significantly enhanced by genetic crossing with the strongest loss-of-function allele of *ter94* (6.5 ± 0.5, Fig. 5C; $P < 0.001$, Fig. 5E). However, there were no significant differences in the size of synaptic boutons among these genotypes (Fig. 5F).

Conversely, the total branch length was significantly longer in the larvae with *ter94* overexpression in the background of neuron-specific *Caz*-knockdown (elav>UAS-*Caz*-IR/UAS-*ter94*, Fig. 5H and I) than in responder control larvae (elav>UAS-*Caz*-IR/UAS-*GFP*, Fig. 5G; 110.7 ± 12.0 versus 54.7 ± 2.5 μm, $P < 0.001$, Fig. 5J). The total branch length in the larvae carrying elav>UAS-*Caz*-IR/UAS-*GFP* was also significantly decreased compared with those carrying *elav/+* (94.4 ± 8.0 versus 54.7 ± 2.5 μm, $P < 0.001$, Fig. 5J). However, there were no significant differences about the total branch length between the larvae carrying *elav/+* and elav>UAS-*Caz*-IR/UAS-*ter94* (Fig. 5J). These results indicated that a loss-of-function *ter94* mutation and wild-type *ter94* overexpression have opposite effects on the synaptic terminal growth and morphogenesis that is impaired by *Caz*-knockdown. Notably, in the larvae with *ter94* overexpression in the background of neuron-specific *Caz*-knockdown (elav>UAS-*Caz*-IR/UAS-*ter94*), the extent of increase in the total branch length showed considerable variability (Fig. 5H and I). Of the larvae with *ter94* overexpression in the background of neuron-specific *Caz*-knockdown, 28% had branch lengths (Fig. 5I) that were 2-fold or more elongated relative to the responder controls (Fig. 5G). The larvae carrying elav>UAS-*Caz*-IR/UAS-*ter94* (Fig. 5H and I) also showed significantly increased number of synaptic boutons of MN terminals (25.6 ± 3.5) compared with those carrying elav>UAS-*Caz*-IR/UAS-*GFP* (8.7 ± 0.5, Fig. 5G; $P < 0.001$, Fig. 5K). The number of synaptic boutons in the larvae carrying elav>UAS-*Caz*-IR/UAS-*GFP* was also significantly decreased compared with that of those carrying *elav/+* (8.7 ± 0.5 versus 14.7 ± 1.0, $P < 0.01$, Fig. 5K). The number of synaptic boutons in the larvae carrying elav>UAS-*Caz*-IR/UAS-*ter94* was significantly increased compared with that of those carrying *elav/+* (14.7 ± 1.0 versus 25.6 ± 3.5, $P < 0.05$, Fig. 5K). The number of synaptic boutons of MNs might be increased in

the larvae carrying elav>UAS-*Caz*-IR/UAS-*ter94* due to the growth of synaptic terminals. There were no significant differences in the size of synaptic boutons among these genotypes (Fig. 5L). These results indicated that Caz is required for growth of MN terminals and formation of synaptic boutons at the NMJ, and these functions of Caz at the MN terminals are affected by the levels of ter94 protein.

DISCUSSION

Here, we demonstrated that eye-specific and neuron-specific *Caz*-knockdown induced a rough-eye phenotype and locomotive dysfunction, respectively; moreover, the locomotive dysfunction was due to the degeneration of MNs. The strongest loss-of-function allele of *ter94* ($ter94^{k15502}$) enhanced such rough-eye and locomotive-dysfunction phenotypes induced by *Caz*-knockdown. Conversely, the overexpression of wild-type *ter94* significantly suppressed the phenotypes induced by *Caz*-knockdown such as rough-eye phenotype, locomotive disabilities and degeneration of MNs. Moreover, neuron-specific *Caz*-knockdown decreased Caz levels in nuclei, and overexpression of wild-type *ter94* significantly suppressed the effects on nuclear *Caz*-expression levels induced by *Caz*-knockdown.

VCP is a member of the AAA protein family; these proteins are involved in diverse cellular functions and in a variety of physiological processes such as cell cycle regulation, membrane fusion, ER-associated degradation, ubiquitin-mediated protein degradation and nucleocytoplasmic shuttling (22–24). VCP is implicated in various neurodegenerative disorders. Mutations in the human *VCP* gene have been reported to cause frontotemporal dementia associated with IBMPFD or familial ALS, and VCP is consequently now considered as a causative gene for FTLD/ALS (25,26). Additionally, previous studies demonstrated that VCP is a binding partner of polyglutamine (polyQ) disease proteins with expanded polyQ tracts (huntingtin, ataxin-1, ataxin-3, ataxin-7 and androgen receptor) (32,33). Previously, the *Drosophila* ortholog of *VCP*, *ter94*, was identified in a screen for genetic modifiers of the eye degeneration phenotypes induced by eye-specific expression of an expanded polyQ tract (34). Moreover, VCP may be involved in diseases that are caused by changes in protein conformation; notably, VCP has been shown to colocalize with pathological protein aggregates in cases of Parkinson's disease, dementia with Lewy bodies, superoxide dismutase 1-associated ALS and Alzheimer's disease (32,35–37).

Our results demonstrate, for the first time, a genetic link between *Caz* and *ter94*, the *Drosophila* orthologs of *FUS* and *VCP*, respectively. Although it would be necessary to confirm whether that is *Drosophila*-specific or not, our results suggest genetic interaction between *FUS* and *VCP* in human. Genetic interaction between TDP-43 and VCP in *Drosophila* was demonstrated previously; IBMPFD-causing mutations in *ter94* lead to redistribution of TDP-43, from the nucleus to the cytoplasm, and redistribution of TDP-43 is sufficient to induce morphologically aberrant rough eyes (24). This previous report suggests that VCP can balance the amount of TDP-43, which is a constituent of larger heteronuclear ribonucleoprotein (hnRNP) complexes, between nucleus and cytoplasm by acting as a nucleocytoplasmic shuttling molecule (Fig. 6). In this schema, VCP functions to remove TDP-43 from RNP complexes, import TDP-43 into nuclei and degrade TDP-43 via autophagy (24,38,39). VCP might have similar functions with respect to FUS because FUS and TDP-43 have significant structural and functional similarities and are implicated in similar molecular processes (40–42). For example, TDP-43 and FUS act in the context of larger hnRNP complexes. FUS also continuously moves between the nucleus and the cytoplasm (16,17,43,44); therefore, FUS not only regulates gene expression in the nucleus, but also has important functions in the cytoplasm (5). Here, we showed that the decreased level of Caz in the nucleus and the resultant motor disturbance induced by neuron-specific *Caz*-knockdown could be rescued by overexpressed wild-type *ter94* despite lacking any change of Caz protein in the CNS (Supplementary Material, Fig. S1A and B). If VCP has a shuttling function as shown in Figure 6, wild-type ter94 overexpression could translocate Caz from cytoplasm to nucleus because nuclear importing function of ter94 would be dominantly induced in the situation with the deficiency of Caz in the nucleus. Conversely, the loss-of-function allele of *ter94* ($ter94^{k15502}$) exacerbated the depletion of *Caz* from the nucleus probably because ter94-mediated nuclear import of Caz was compromised.

It has been demonstrated that a polyQ tract can interact with VCP in *Drosophila* (34); specifically, either the strongest ($ter94^{k15502}$) or strong ($ter94^{03775}$) loss-of-function allele of *ter94* suppressed the eye degeneration induced by an expanded polyQ tract, whereas the overexpression of wild-type *ter94* in the background of *Caz*-knockdown enhanced this phenotype. Additionally, a chromosomal deletion of 46C3–46E02, the genomic region that contains *ter94*, acted as a dominant suppressor of the polyQ-induced phenotype (34). Our present study and these previous reports together indicate that gain and loss of *ter94* function rescued and exacerbated *Caz*-knockdown phenotypes, respectively, and that they had the converse effects on polyQ-induced phenotypes. These converse effects could be explained by the difference in disease pathogenesis; in polyQ-induced disease models, polyQ-containing pathogenic aggregates exist in nuclei of affected neurons; in contrast, Caz expression in nuclei is deficient in *Caz*-knockdown disease models. Overexpression of wild-type *ter94*, which functions in nuclear import of polyQ or Caz, would exacerbate nuclear polyQ aggregation, but could alleviate the nuclear deficiency of Caz protein.

Neuron-specific *Caz*-knockdown flies showed an age-dependent decline in climbing ability that was significantly worse than driver control flies for every age examined after day 7. Overexpression of wild-type *ter94* significantly rescued the declined locomotor ability caused by *Caz*-knockdown up to day 14, but it did not rescue the phenotype at later stages. Regarding the age-dependent ability to rescue locomotive deficits, we considered the two following possible explanations. First, the elongation of the branch length of MN terminals at NMJs caused by overexpression of wild-type *ter94* in neuron-specific *Caz*-knockdown flies may have alleviated the locomotive defects caused by neuron-specific *Caz*-knockdown. However, the extent of this elongation was highly variable. A previous report showed that larvae with NMJ overgrowth phenotypes exhibited mobility defects; this finding indicates that the elongation of nerve terminal branches beyond some adequate

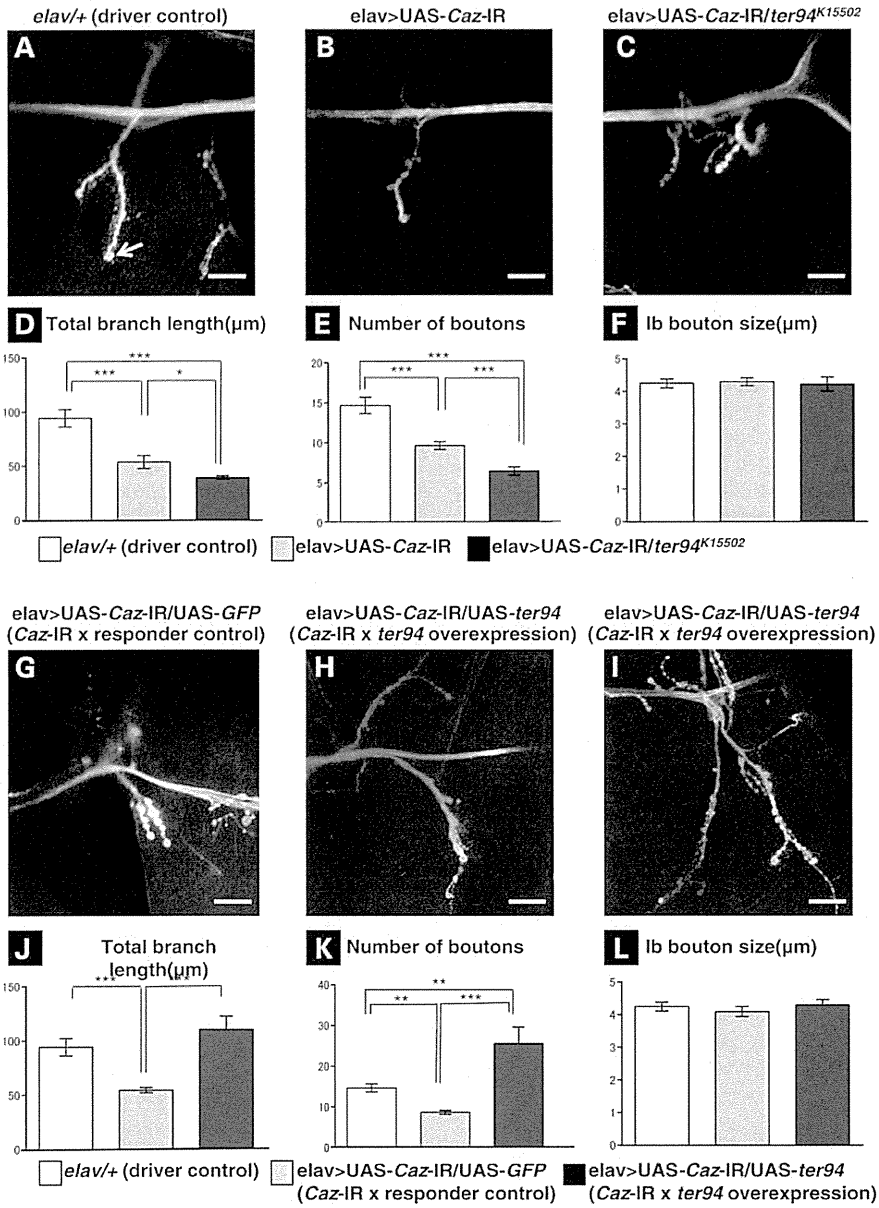

Figure 5. A loss-of-function *ter94* mutation and wild-type *ter94* overexpression change the morphology of MN presynaptic terminals in the NMJ of MN4 in neuron-specific *Caz*-knockdown larvae in opposite ways. A representative image of anti-horseradish peroxidase staining of muscle 4 synapses in third instar larvae with *elav/+* (**A**; a driver control), neuron-specific *Caz*-knockdown (**B**; elav>UAS-*Caz*-IR), neuron-specific *Caz*-knockdown crossed with the strongest loss-of-function mutation of *ter94* (**C**; elav>UAS-*Caz*-IR/*ter94*^{K15502}), neuron-specific *Caz*-knockdown crossed with UAS-*GFP* (**G**; elav>UAS-*Caz*-IR/UAS-*GFP*; a responder control) or neuron-specific *Caz*-knockdown crossed with UAS-*ter94* (**H** and **I**; different larvae with the same genotype, elav>UAS-*Caz*-IR/UAS-*ter94*). (**D** and **J**) Total branch length of the NMJ from muscle 4 for each of the indicated genotypes. Compared with the total length of synaptic branches of MNs in driver control larvae (A), that in neuron-specific *Caz*-knockdown larvae (B) is significantly decreased ($P < 0.001$, $n = 10$, D). This decrease in branch length observed in the neuron-specific *Caz*-knockdown larvae (B) is significantly worsened in larvae carrying the strongest loss-of-function allele of *ter94* and neuron-specific *Caz*-knockdown (C) ($P < 0.05$, $n = 10$, D). Conversely, the total branch length in larvae that overexpressed wild-type *ter94* in the background of neuron-specific *Caz*-knockdown (H and I) is significantly longer than that in larvae carrying elav>UAS-*Caz*-IR/UAS-*GFP* (G) ($P < 0.001$, $n = 14$, J). The extent of increase in the total branch length of elav>UAS-*Caz*-IR/UAS-*ter94* was highly variable among individual flies (H and I). The total branch length of synaptic branches of MNs in the larvae carrying elav>UAS-*Caz*-IR/UAS-*GFP* is significantly decreased compared with that of larvae carrying *elav/+* ($P < 0.001$, $n = 12$, J). (**E** and **K**) The number of synaptic boutons for each of the indicated genotypes. The number of synaptic boutons of MNs in neuron-specific *Caz*-knockdown larvae (B) is also significantly decreased compared with driver control larvae (A) ($P < 0.001$, $n = 10$, E). This decrease in the number of synaptic boutons in the neuron-specific *Caz*-knockdown larvae is significantly worsened in larvae carrying the strongest loss-of-function allele of *ter94* and neuron-specific *Caz*-knockdown (C) ($P < 0.001$, $n = 10$, E). Conversely, the number of synaptic boutons in the larvae carrying wild-type *ter94* overexpression in the background of neuron-specific *Caz*-knockdown (H and I) is significantly higher than that in responder control larvae (G) ($P < 0.001$, $n = 10$, K). Compared with the larvae carrying *elav/+*, the number of synaptic

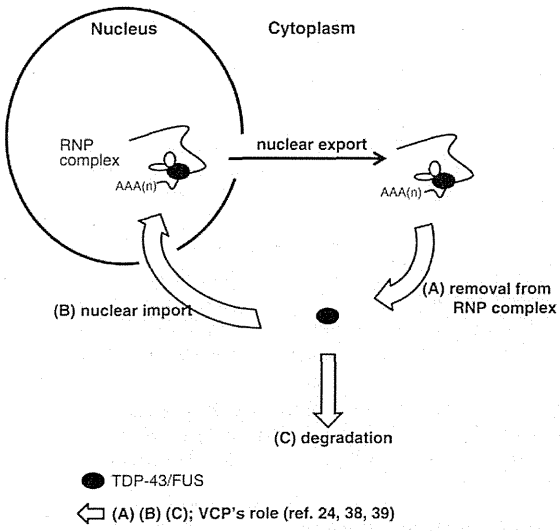

Figure 6. Hypothetical roles of VCP in the nucleoplasmic balance of TDP-43 and FUS referring to the paper by Ritson *et al.* (24). VCP, human ortholog of ter94, may act during removal of TDP-43/FUS from RNP complexes in the cytoplasm (**A**), nuclear import of TDP-43/FUS (**B**) and degradation of TDP-43/FUS by the autophagic pathway (**C**). FUS, the human ortholog of Caz, might translocate from cytoplasm to nucleus when VCP is overexpressed because the nuclear-import function of VCP (B) would be dominantly induced under conditions of FUS deficiency in nuclei. Conversely, loss-of-function alleles of VCP may exacerbate the FUS deficiency in nuclei because FUS is not being properly imported into nuclei by VCP.

length could cause disturbances in locomotive ability (45). Therefore, synaptic MN terminals may have to be within some optimal range of lengths. Second, the age-dependence of ability to rescue the locomotive defects might be due to the age-dependent difference in the expression levels of ter94. Tissue expression data from FlyBase (http://flybase.org) show that mRNA expression levels of *ter94* are very high in the CNS of third instar larvae, but they are relatively low in the head, eye or brain of adults. Age-dependent changes in ter94 expression levels might determine the period within which wild-type ter94 overexpression can rescue locomotive deficits caused by *Caz*-knockdown. Age-dependent effects of ter94 are also evident in fly models of polyQ-induced neurodegeneration. Between the third instar larval stage and the late pupal stage, levels of ter94 were elevated, and elevated levels of ter94 induced severe apoptotic cell death in those pupae (34).

In some IBMPFD-associated VCP mutants, it was previously reported that pathogenic VCPs could bind to cofactors, such as Npl4, Ufd1 or p47, more efficiently than wild-type VCP (46,47). However, little is known about which of the VCP cofactors relate to FUS-nuclear translocation or how the conformational change of VCP affects the interactions of VCP cofactors with other proteins.

In conclusion, we found a genetic interaction between *Caz* and *ter94*. Our data indicate that chemicals that up-regulate the function of VCP or facilitate nuclear import of FUS may suppress the pathogenic processes that lead to the degeneration of MNs in FUS-associated ALS/FTLD. This might be the first step to develop candidate drugs for the disease-modifying therapy of human ALS.

MATERIALS AND METHODS

Fly stocks

Fly stocks were maintained at 25°C on standard food containing 0.7% agar, 5% glucose and 7% dry yeast. Canton S was used as the wild-type strain. The strain: w^{1118}; *P {w [+mC] = UAS-GFP. nls} 14* (DGRC number 107870) (UAS-*GFP*) and chromosomal deficiency line: *Df (2R) X1*, $Mef2^{X1}$/*CyO*, Adh^{nB} (DGRC number 106718) were obtained from the Kyoto *Drosophila* Genetic Resource Center. The strains: *w* [*]; *P {[+mC] = GAL4-elav.L} 3* (Bloomington BL8760) (*elav-GAL4*), y^1w [*]; *P {[+mC] = Act5C-GAL4} 17bFO1/TM6B*, Tb^1 (BL3954) (*Act5C-GAL4*), y^1w^{67c23}; *P {w [+mC] = lacW} ter94*^{K15502}/*CyO* (BL10454) (*ter94*^{K15502}) and cn^1P {*ry* [+*t7.2*] = *PZ*} *ter94*^{03775}/*CyO*; ry^{506} (BL11349) (*ter94*^{03775}) were obtained from the Bloomington *Drosophila* stock center in Indiana. Establishment of the lines carrying *GMR-GAL4* was as described previously (48). We crossed transgenic UAS-*Caz*-IR flies with *Act5C-GAL4*, *GMR-GAL4* or *elav-GAL4* flies to drive expression of *Caz* dsRNA throughout the whole body of flies, specifically in eye imaginal discs or specifically in neuronal tissues, respectively. We generated eye-specific *Caz*-knockdown flies (*GMR-GAL4*; UAS-*Caz*-IR/+; +) (GMR>UAS-*Caz*-IR) and neuron-specific Caz-knockdown flies (w; UAS-*Caz*-IR/+; *elav-GAL4*/+) (elav>UAS-*Caz*-IR). Each transgenic strain showed a consistent phenotype (Table 1).

Dr Kakizuka kindly provided UAS-*ter94* flies. The UAS-*ter94*-IR strain: w^{1118}; *P {GD9777} v24354* (VDRC number v24354) (*ter94*-knockdown) was obtained from the VDRC. VDRC reports that the *ter94*-RNAi construct is inserted into chromosome 2 and has no off-target effects. The lines generated in this study are as follows: *GMR-GAL4*; +; + (*GMR*), *GMR-GAL4*; UAS-*Caz*-IR363−399/+; + (GMR>UAS-*Caz*-IR), *GMR-GAL4*; UAS-*Caz*-IR363−399/UAS-*Caz*-IR363−399; + (GMR>UAS-*Caz*-IR/UAS-*Caz*-IR), *GMR-GAL4*; UAS-*Caz*-IR363−399/*ter94*^{K15502}; + (GMR>UAS-*Caz*-IR/*ter94*^{K15502}), *GMR-GAL4*; UAS-*Caz*-IR363−399/*ter94*^{03775}; + (GMR>UAS-*Caz*-IR/*ter94*^{03775}), *GMR-GAL4*; UAS-*Caz*-IR363−399/UAS-*GFP*; + (GMR>UAS-*Caz*-IR/UAS-*GFP*), *GMR-GAL4*; UAS-*Caz*-IR363−399/UAS-*ter94*; + (GMR>UAS-*Caz*-IR/UAS-*ter94*), w; +; *elav-GAL4*/+ (*elav*/+; a driver control), UAS-*Caz*-IR363−399/+ (UAS-*Caz*-IR/+; a responder control), *ter94*^{K15502}/+, w; UAS-*Caz*-IR363−399/+; *elav-GAL4*/+ (elav>UAS-*Caz*-IR), w; UAS-*Caz*-IR363−399/UAS-*Caz*-IR363−399;

boutons is significantly decreased in the larvae carrying elav>UAS-*Caz*-IR/UAS-*GFP* ($P < 0.001$, $n = 10$, K), but significantly increased in those carrying elav>UAS-*Caz*-IR/UAS-*ter94* ($P < 0.05$, $n = 14$, K). (**F** and **L**) The size of synaptic boutons for each of the indicated genotypes. The size of Ib bouton (indicated with an arrow in A) was measured ($n = 31$ for *elav*/+, $n = 33$ for elav>UAS-*Caz*-IR, $n = 31$ for elav>UAS-*Caz*-IR/*ter94*^{K15502}, $n = 30$ for elav>UAS-*Caz*-IR/UAS-*GFP* and $n = 32$ for elav>UAS-*Caz*-IR/UAS-*ter94*). There are no significant differences in the size of synaptic boutons among driver control larvae, either larvae with elav>UAS-*Caz*-IR and those with elav>UAS-*Caz*-IR/*ter94*^{K15502} (F) or among driver control larvae, either larvae with elav>UAS-*Caz*-IR/UAS-*GFP* and elav>